Impacts of Vegetation on Dryland River Morphology: Insights from Spring-Fed Channel Reaches, Henry Mountains, Utah

Paul J. Southard[1], Joel P. L. Johnson[2], Daniella Rempe[3], and Ashley M Matheny[2]

[1]The University of Texas at Austin
[2]University of Texas at Austin
[3]University of Texas at Austinn

November 23, 2022

Abstract

A better understanding of how vegetation influences alluvial channels could improve (a) assessments of channel stability and flood risks, (b) applications of vegetation as a river management tool, and (c) predictions of channel responses to climate change and other human impacts. We take advantage of a natural field experiment in the semi-arid to arid Henry Mountains, Utah, USA: Large spatial differences in bed and bank vegetation are found along some alluvial channels due to localized perennial springs caused by aquicludes in the underlying bedrock. Airborne LiDAR topography and flood modeling are used to constrain channel morphology, vegetation density, and flow velocity at different flood discharges for three spring-fed reaches along intermittently-flowing streams. The spatial distribution of vegetation quantitatively influences both the magnitude and direction of channel adjustment. Reaches with abundant *bed* vegetation are significantly wider (by an average of [?] 50%), with shallower flows and lower velocities, than reaches with little bed vegetation. Reaches with dense channel *bank* vegetation are [?] 25% narrower and [?] 25% deeper than sparsely-vegetated reaches. We interpret that sediment grain size influences the spatial distribution of vegetation within spring reaches, but that bank vegetation may be more important than grain size for "threshold" width adjustments. Widths, depths and velocities are fairly insensitive to whether local hydraulic roughness is parameterized in terms of local vegetation density or is assumed spatially constant, suggesting that the underlying "bare earth" topography of the channel bed, banks and floodplain exerts more control on local flow than does local vegetation density.

Hosted file

`southard_etal_supportinginfo112721.docx` available at https://authorea.com/users/543200/articles/601192-impacts-of-vegetation-on-dryland-river-morphology-insights-from-spring-fed-channel-reaches-henry-mountains-utah

Impacts of Vegetation on Dryland River Morphology: Insights from Spring-Fed Channel Reaches, Henry Mountains, Utah

P. J. Southard[1], J. P. L. Johnson[1*], D. M. Rempe[1], A. M. Matheny[1]

[1]Department of Geological Sciences, Jackson School of Geosciences, The University of Texas at Austin, Austin, TX, USA

[*]Corresponding author: Joel P. L. Johnson (joelj@jsg.utexas.edu)

Key Points

- Groundwater-fed springs in dryland landscapes provide an opportunity to isolate effects of vegetation on channel morphodynamics.
- Vegetation can drive channel widening or narrowing, depending on whether the vegetation is focused on the channel bed or banks.
- Sediment size distribution, an absence of base flow, and water availability control whether riparian vegetation stabilizes channel beds.

Keywords: Channel Morphology; Riparian Vegetation; Hydraulic Geometry; Ephemeral flow; Dryland; Flow Modeling; Channel Bed Vegetation; Channel Bank Vegetation; Hydraulic Roughness; Morphodynamics

Abstract

A better understanding of how vegetation influences alluvial channels could improve (a) assessments of channel stability and flood risks, (b) applications of vegetation as a river management tool, and (c) predictions of channel responses to climate change and other human impacts. We take advantage of a natural field experiment in the semi-arid to arid Henry Mountains, Utah, USA: Large spatial differences in bed and bank vegetation are found along some alluvial channels due to localized perennial springs caused by aquicludes in the underlying bedrock. Airborne LiDAR topography and flood modeling are used to constrain channel morphology, vegetation density, and flow velocity at different flood discharges for three spring-fed reaches along intermittently-flowing streams. The spatial distribution of vegetation quantitatively influences both the magnitude and direction of channel adjustment. Reaches with abundant *bed* vegetation are significantly wider (by an average of ≈ 50%), with shallower flows and lower velocities, than reaches with little bed vegetation. Reaches with dense channel *bank* vegetation are ≈ 25% narrower and ≈ 25% deeper than sparsely-vegetated reaches. We interpret that sediment grain size influences the spatial distribution of vegetation within spring reaches, but that bank vegetation may be more important than grain size for “threshold” width adjustments. Widths, depths and velocities are fairly insensitive to whether local hydraulic roughness is parameterized in terms of local vegetation density or is assumed spatially constant, suggesting that the underlying “bare earth” topography of the channel bed, banks and floodplain exerts more control on local flow than does local vegetation density.

Plain Language Summary

Vegetation is found almost everywhere on Earth’s surface and varies with regional climate rather than over short distances. It is therefore difficult to isolate how vegetation influences river channel dimensions from other controls such as flood discharges or sediment grain size, or to predict how climate change may drive river change. We isolate vegetation controls by studying river channels with large natural variations in vegetation due to localized groundwater springs. We use high resolution topographic data (collected using lasers shot from airplanes) to measure how much vegetation is found along and in channels, and we use computer models to calculate the width, depth and velocity of flow at different flood discharges. We find that vegetation can

cause channels to either be narrower or wider, depending on whether more vegetation is focused on channel beds or banks, and we quantify the magnitude of these effects.

1. Introduction

Riparian vegetation is present in essentially all terrestrial fluvial environments, and influences alluvial channel morphology through feedbacks with flow and sediment transport (e.g., Bywater-Reyes et al., 2017; Camporeale et al., 2013; Gurnell, 2013; Hickin, 1984; Manning et al., 2020; Milan et al., 2020; Osterkamp & Hupp, 2010; Wiel & Darby, 2013). Vegetation can reduce bed and bank erodibility through root strength; it also imparts drag on flow but can enhance local turbulence and scour (e.g., Corenblit et al., 2007; Fischenich, 1997; Gran & Paola, 2001; Gurnell, 2014; Micheli and Kirchner, 2002a,b; Nepf, 1999; Smith, 1976; Yager and Schmeeckle, 2013). Vegetation covaries with other variables that affect channel form including climate, land use, disturbance history, and soil characteristics. Understanding these feedbacks is necessary for predicting channel responses to climate change or anthropogenic disturbances (Corenblit & Steiger, 2009; Dean and Topping, 2019; Gurnell et al., 2015), and for modifying riparian vegetation for river management (Andreoli et al., 2020; González et al., 2015; Vargas-Luna et al., 2018). However, effects of vegetation are difficult to isolate because of the very pervasiveness and complexity of vegetation-related feedbacks (e.g., Osterkamp & Hupp, 2010; Simon & Collison, 2002).

In rivers with persistent baseflow, water availability tends to promote bank vegetation but prevent bed vegetation. Field studies have demonstrated that dense bank vegetation causes channels to narrow and deepen, and can influence planform morphology (Friedman et al., 1996; Graf, 1978; Hey & Thorne, 1986; Huang & Nanson, 1997; Millar, 2000; Perignon et al., 2013). Graf (1978) exploited temporal variation in vegetation density, caused by the establishment of tamarisk on the Green River, to determine that growth of bank vegetation caused a 27% reduction in mean width. Micheli and Kirchner (2002b) measured vegetated bank strengths using a large shear vane, and showed that channels with stronger vegetated banks migrated laterally more slowly. Laboratory experiments using alfalfa have demonstrated that floodplain vegetation can cause transitions from braided to single-threaded channels, and enhance meander migration rather than avulsion by choking off secondary channels (Braudrick et al., 2009; Gran and Paola, 2001; Tal and Paola, 2007, 2010; Tal et al., 2013). Numerical models that account for flow resistance and bank strength from vegetation capture similar effects on baseflow (e.g., Crosato and Saleh, 2011; Murray and Paola, 2003).

Although dryland landscapes comprise over 40% of Earth's terrestrial surface (Millennium Ecosystem Assessment, 2005), river dynamics in these systems are less studied than in wetter landscapes with baseflow (e.g., Gurnell, 2014). Even in exceedingly dry regions, subsurface water availability is highest near river channels, supporting vegetation (Hupp & Osterkamp, 1996). In intermittently flowing streams, channel bed vegetation can have time to establish itself during periods between major floods (Coulthard, 2005; Dunkerly, 1992; Huang & Nanson, 1997). Interestingly, channel bed vegetation can have opposite effects on channel geometry from channel bank vegetation. Several dryland field studies have shown that channels may be wider, with multi-threaded to anabranching patterns, where vegetation is on the channel bed (Pietsch & Nanson, 2011; Wende & Nanson, 1998). Flume experiments by Coulthard (2005) found that braiding index increases as channel bed plant density increases. Of particular relevance to our analysis, Huang and Nanson (1997) used four dryland Australian channels to quantify how channel width, depth, and flow velocity were different depending on whether vegetation was present on channel banks only, or on both banks and bed. Some of their channel reaches were sand-bedded, and some gravel-bedded, with trees and shrubs as the dominant vegetation. They found (a) that bankfull width was ≈ 1.6-2 times wider in reaches with both *bed and bank vegetation (B&BV)* compared to *bank-only vegetation (BOV)*, and narrower in reaches with dense *BOV* compared to little *BOV*, (b) that calculated flow velocity was ≈2.7 times slower in reaches with *B&BV* but insensitive to the amount of *BOV*, and (c) that depth was relatively insensitive to *B&BV*, but increased with dense *BOV*.

We frame our work around two overall hypotheses. First, we broadly predict that channel morphology (e.g., combinations of width, depth, and slope) and flow velocity vary systematically with metrics of local channel vegetation. Second, we specifically hypothesize that the above quantitative relations found by Huang and Nanson (1997) will also hold true for our

Henry Mountains channel reaches. Testing these hypotheses will help evaluate the universality of empirical relations predicting how vegetation influences dryland channels.

2. Study area: Henry Mountains, Utah, USA

In the Henry Mountains of southern Utah, channels with springs provide a natural laboratory for studying the impact of riparian vegetation on channel morphology (Figure 1; Gilbert, 1877; Hunt et al., 1953). Based on our field observations these springs provide enough water to support local vegetation, but with negligible surface flow. Most spring discharge remains in the local subsurface alluvium. We focus on two channels: Woodruff Canyon, which has an upper and lower spring, and Trail Canyon, which has one spring (Figure 1). Spring locations are lithologically controlled. The Trail Canyon spring and Lower Woodruff Spring occur at the contact between the permeable eolian Navajo Sandstone (Jn) above and the Kayenta formation (Jk) below (which has aquicludes from abundant mud and silt layers that are interbedded with coarse fluvial sands). The upstream Woodruff Spring occurs at the contact between the permeable and predominantly eolian Entrada Sandstone above (Je) and the Carmel formation (Jca) below (a shallow marine mudstone with gypsum lenses). While small areas of bedrock are occasionally exposed along these channels in the bed or banks, for this study we treat the channels as alluvial because the bed and banks of the reaches we study are alluvial, and the vegetation is rooted into alluvium. Johnson et al. (2009) surveyed ≈ 2% bedrock exposure in the bed and banks of a longer Trail Canyon section. Ouimet et al. (2008) documented narrow bedrock-walled locations along lower Trail Canyon which we exclude from our analysis.

Sediment grain size distributions (GSDs) vary substantially in different Henry Mountains channels, because of spatial variability in coarse sediment that is eroding from older localized pediment remnants and from igneous intrusions outcropping upstream in some but not all watersheds in the area (Johnson et al., 2009). GSDs were measured by random-walk point counts (corresponding to “grid by number”, Kellerhals and Bray, 1971). Trail Canyon is significantly coarser than Woodruff Canyon (see Results).

The drainage area is ≈4.5 km^2 at upper Woodruff spring, and ≈20 km^2 at the springs in both lower Woodruff and Trail canyons. Discharge primarily occurs from localized North American monsoon storms in July-October, although we have observed minor snowmelt flow in some years. We have also observed that flow from storms at higher elevations in the channel often does not reach lower channel elevations before infiltrating into the dry riverbed. While ungauged, field observations demonstrate that these and similar channels do not flow the vast majority of the time (Johnson et al., 2009, 2010). Mean annual precipitation (MAP) at all three spring locations is 20-21 cm/year (PRISM Climate Group, 2021). The highest elevations of the Woodruff watershed reach 26 cm/yr MAP. The Trail Canyon watershed reaches significantly higher elevations and has a maximum MAP of 64 cm/yr, although it should be noted that over half of the high-elevation precipitation falls as snow in winter months.

Away from the springs, channel banks and occasionally beds are sparsely vegetated in places with drought-tolerant trees such as Utah Juniper (*Juniperus osteosperma*) and Fremont Cottonwood (*Populus fremontii*) and woody shrubs such as Desert Sage (*Salvia dorrii*), Brigham Tea (*Ephedra nevadensis*), Creosote (*Larrea tridentata*), Sagebrush (*Artemisia tridentata*), Rabbitbrush (*Chrysothamnus* spp.), and Utah Yucca (*Yucca utahensis*), which we infer to reflect water-limited conditions (Figure 1b, d, f). In contrast, reaches at and immediately downstream of the springs have dense vegetation, consisting of grass, reeds, horsetails, woody shrubs (Shrub Live Oak (*Quercus turbinella*)), herbaceous shrubs, and trees (Fremont Cottonwood, Quaking Aspen (*Populus tremuloides*) (Figure 1c, e, g).

3. Methods

4.1 Study design

Our methods are designed to objectively measure channel characteristics, and to isolate vegetation variables from other factors that can influence channel form. Natural, systematic, and persistent variations in riparian vegetation are rarely found along the same channel over distances short enough that other controls on morphology (e.g., local climate, channel slope and drainage area, discharge, sediment supply, perturbation histories) remain fairly constant. A relatively unique advantage of our field site is that large natural differences in vegetation are found along individual channel reaches over short distances (≈100 m or less). Importantly, we can assume that the history of flood discharges must be the same for adjacent reaches with different amounts of vegetation along the same channel. Similarly, over timescales encompassing many floods the sediment flux and size distribution moving through adjacent reaches must be comparable, as there are no indications of systematic differences in aggradation or degradation. We also assume that the lithologically-controlled locations of springs have been consistent over timescales longer than are required for vegetation and alluvial channel form to adjust to hydrologic conditions. A limitation of our field site is that the channels are all ungauged, and so we do not know the actual distributions of discharge, flood recurrence intervals, or sediment transport rates.

Our study is limited to three reaches, 1.4 to 7.8 km in length, with small changes in drainage area along each reach. We objectively quantify channel geometry at different calculated discharges by combining airborne LiDAR topography with numerical flow modeling. LiDAR data provide quantitative estimates of vegetation density, canopy height, and bare earth topography. 2D flow modeling allows for objective measures of wetted cross-sectional geometry at a given imposed discharge. Although we were only able to evaluate three channel reaches with variable vegetation, the high spatial resolution of the LiDAR data relative to reach lengths allows for robust statistical comparisons.

We compare our analysis of how channel geometry varies with vegetation to that of Huang and Nanson (1997). They conducted field surveys in which they interpreted bankfull width, depth, and slope from channel cross-sectional geometry, for 30 total cross sections along four channels. They estimated hydraulic roughness (Manning's n) by visually comparing their reaches to calibrated photographs (Barnes, 1967), and calculated bankfull discharge based on these constraints. They used these bankfull estimates at different drainage areas to infer downstream hydraulic geometry changes (Leopold and Maddock, 1953). Complementary to Huang and Nanson (1997), our Henry Mountains analysis represents at-a-station hydraulic geometries (Leopold and Maddock, 1953).

4.2 LiDAR processing

We use National Center for Airborne Laser Mapping (NCALM) LiDAR data collected on September 7, 2011, with data points already classified as "ground" or as "unclassified" (Olinde, 2012). The average point density for this dataset is 5.07 pts/m^2. Unclassified points tended to be roads, very steep bedrock surfaces (e.g. slickrock and canyon sidewalls), and vegetation. As no roads or steep bedrock surfaces occur in our valley bottom reaches, we assume that all points not classified as ground were vegetation (hereafter referred to as "vegetation points"). We used the ArcGIS 10.5 LAS Dataset to Raster tool to create a digital elevation model (DEM) with 1 m spacing from the ground-classified points. To minimize the effect of possible low vegetation misclassified as ground, we used the minimum elevation at each grid cell to represent that elevation.

We propose a simple metric of relative spatial vegetation density called the *LiDAR Vegetation Index (LVI)*. Within a given 1 m grid cell, we divided the number of vegetation points by the total number of points (vegetation and ground) within the cell and define the ratio of the two as *LVI*.

4.3 AnuGA flow modeling and analysis

We used flow modeling to define the channel (wetted) area and measure how width, depth, and velocity varied with discharge. AnuGA is an open-source Python package that uses a finite volume method to solve the depth-averaged shallow water wave equations (i.e. St. Venant) over a triangular irregular mesh (TIN) (Roberts et al., 2015). All simulations were performed with TINs automatically generated by AnuGA from the bare earth LiDAR DEMs, with a maximum triangle area of 1 m^2. We simulated 10, 20, 30, 40 and 50 m^3/s flood discharges in each channel, imposed at the upstream boundary. Because the channels are ungauged we do not have constraints on recurrence intervals corresponding to these discharges. Instead, these flows were chosen because preliminary modeling indicated that they spanned the range of discharges from being contained within all of the study reaches to overbank flows, and were consistent with discharges calculated by Huang and Nanson (1997) for similarly sized channels, facilitating direct comparison to their analysis. All models were run until flow was steady, at which point the flood wave had propagated all the way down the channel, the water surface was not changing through time, and the discharge at the downstream boundary matched the upstream discharge. AnuGA's SWW2DEM tool was used to create rasters of depth and velocity at steady state flow. We note that the way discharge was imposed at the upstream modeled cross section, combined with numerical rounding and cross section interpolation, led to relatively small differences in modeled discharge between runs and cross sections (Table 1). More details of the analysis are provided in Southard (2019).

Sets of flow models were completed using two different hydraulic roughness assumptions, which we interpret as end-member bounds for understanding how vegetation density influences flow characteristics and channel morphology. First, we assumed a spatially constant Manning's *n* of 0.04, based on the similarity of photographs and descriptions from Barnes (1967) to our sparsely-vegetated reaches with relatively high roughness from bed sediment and topography, but not primarily from vegetation. Uniformly applying n=0.04 regardless of local vegetation variability was done to better isolate the effects of local topography on width, depth, and velocity at a given discharge. This calculation (a) serves as a minimum bound on the influence of vegetation on channel form (i.e., without yet considering additional localized drag from vegetation), and (b) ensures that comparisons of flow characteristics to vegetation density are not biased by having flow calculations be functions of vegetation density.

Second, we also calculated flow using spatially variable hydraulic roughness parameterized from vegetation-classified LiDAR returns. Following Abu-Aly et al. (2014) we adapted a method from Casas et al. (2010), who incorporated LiDAR-based canopy heights into equations from Katul et al. (2002) based on physical experiments and a mixing layer theory for shallow streams. Roughness depended on the canopy height and flow depth at each cell:

$$n = \frac{h^{\frac{1}{6}}}{\sqrt{g} C_u f(\xi, \alpha)} \tag{1}$$

$$\xi = \frac{h}{V_{ch}} \tag{2}$$

$$f(\xi, \alpha) = 1 + \frac{\alpha}{\xi} ln \left[\frac{\cosh\left(\frac{1}{\alpha} - \frac{1}{\alpha}\xi\right)}{\cosh\left(\frac{1}{\alpha}\right)} \right] \tag{3}$$

where h is water depth, V_{ch} is LiDAR-derived average vegetation canopy height at a given location, C_u is a similarity constant, α is the characteristic eddy size coefficient, and g is gravity.

Casas et al. (2010) empirically estimated $C_u = 4.5$ and $\alpha = 1$. We used h corresponding to a given discharge from the uniform roughness flow models. From the vegetation-classified LiDAR point cloud we calculated V_{ch} as the average canopy height of all vegetation returns within each raster cell. Following Abu-Aly et al. (2014), we did not include the additional Casas et al. (2010) parameterization of sub-grid roughness from LiDAR data.

Abu-Aly et al. (2014) implemented equation (1) cell-by-cell to estimate roughness wherever $0.2 < \xi < 7$, the range over which it is approximately appropriate to assume a logarithmic boundary layer velocity profile (Casus et al., 2010; Katul et al., 2002). Where $\xi > 7$ (vegetation much shorter than the flow depth) or $\xi < 0.2$ (trees making canopy height much taller than the flow depth), they assigned *n*=0.04 (the substrate roughness). Where $\xi > 7$, we set *n*=0.04, consistent with Abu-Aly et al. (2014). For $1 \leq \xi \leq 7$ we used equations (1-3) to calculate *n*. We set $\xi = 1$ as the minimum ξ value (i.e., $\xi < 1$ were set to 1), because $\xi < 1$ resulted in some unrealistically high values of $n > 0.2$. Setting our lower limit to ξ=1 resulted in maximum cross-section *n* ranging from 0.1 to 0.14. Because densely-vegetated sections in Upper and Lower Woodruff Canyon were more vegetated than the roughest example (*n*=0.075) in Barnes (1967), we used the Arcement and Schneider (1967) visual guide for floodplain roughness to independently estimate that the most densely-vegetated reaches likely have $n \approx 0.11$-0.15, consistent with our lidar-based analysis. In comparison, Huang and Nanson (1997) used “the procedure of Barnes (1967)” to estimate *n* from 0.021 to 0.14 for their 30 variably vegetated reaches (median n = 0.051, mean n = 0.064, standard deviation σ = 0.033).

We interpreted the flow modeling results in terms of channel cross sections. We calculated the thalweg path along each reach from flow accumulation based on the bare earth DEM. Every 10 m along the thalweg we calculated a channel cross section oriented perpendicular to the thalweg reach. This ultimately resulted in cross section calculations of wetted perimeter, area, depth, hydraulic radius, velocity, and average proportion of vegetation points. Finally, to reduce variability, we averaged the data over a -4 to +4 cross-section moving window resulting in data that represent the average of 90 m of distance along the channel.

4. Results

To provide context for our quantitative analysis, we first present field observations relating vegetation, water availability and channel form. Away from the spring-fed reaches, vegetation was much more abundant on banks and occasional in-channel bars than on the channel bed itself. Morphologically, the minimally-vegetated channel reaches tended to be fairly trapezoidal in cross section, often with a single broad thalweg and sloping banks that were straightforward to define visually. Sparse dryland vegetation was common along the tops of banks and the surrounding floodplain. In the vicinity of all three springs, groundwater seepage was visible at some lithologic aquicludes exposed on canyon walls (Figure 1i).

A short distance upstream of the Trail study reach the median intermediate diameter is D_{50}=5.3 cm, the geometric mean is D_{gm}=3.0 cm, D_{84}=15 cm, and 22% of the bed covered by sand (diameters $\leq$ 2 mm). In Woodruff Canyon (measured in a reach between the two study areas) D_{50}=0.6 cm, D_{gm}=0.9 cm, D_{84}=5.1 cm, with 30% of the bed covered by sand (Supporting Information Figure S1). Both channels have bimodal distributions, with histogram peaks in sand sizes and at 9.8 cm and 4.7 cm for Trail and Woodruff, respectively. Detailed grain size measurements from separate more- and less-vegetated study reaches are unavailable.

5.1 Woodruff Canyon

The upstream transition from sparse to dense vegetation occurred over lengths less than 100 m near both Woodruff springs. In the most densely-vegetated reaches, vegetation covered the entire channel bed and banks (Figure 1c,e) . The downstream transition back to sparse vegetation occurred relatively gradually over streamwise distances of 1/2 - 1 km. Grass and reed abundances declined rapidly over scales of 50-100 m, suggesting greater sensitivity to near-surface water availability, while shrubs and trees appeared to decrease more gradually over hundreds of meters. Channel form correspondingly transitioned. Reaches upstream of the springs had clearly-defined banks with some vegetation, but minimal bed vegetation. In the densely vegetated reaches it was usually difficult to identify distinct breaks between bank and floodplain in the field (Figure 1c, e). Cross sections generally exhibited lower relief than their sparsely-vegetated counterparts upstream, and often had multiple subtle thalwegs. LiDAR topography, with vegetation removed, similarly resolve channel banks bounding a single main channel in the sparsely-vegetated reaches (Figure 2a), but less bank structure and multiple flow paths in densely-vegetated reaches (Figure 2h).

Along both lower and upper Woodruff Canyons, surface water was observed coming out of the alluvium within tens of meters of where dense vegetation started. The surface discharge was extremely low and flow was entirely accommodated by a very small thalweg not resolved by LiDAR data (Figure 1h). The thalweg at each spring was generally less than 20 cm in width, incised as much as 0.5 m into the surrounding channel bed alluvium and had rectangular cross sections with nearly vertical sidewalls supported by root systems. Longitudinal steps, supported by tree roots or cobble-sized clasts, were common along these thalwegs. These narrow thalwegs were the only locations in the vegetated reaches where the persistent presence of water prevented establishment of vegetation. Qualitatively, the surface discharge in each of these channels appeared similar during summer and fall field visits, suggesting that spring discharges are persistent across seasons.

5.2 Trail Canyon

In sparsely-vegetated reaches, some woody shrubs were present on channel banks (Figure 1f). The transition from sparsely-vegetated to densely-vegetated occurred over a length less than 100 m in Trail Canyon. In contrast to Woodruff, the vegetated reach of Trail Canyon had clearly defined and more densely vegetated banks, with little to no vegetation on the channel bed (Figure 1g). Densely-packed shrubs and cottonwoods were present on the channel bank and some shrubs were present on bars within the channel. Unlike the Woodruff spring areas, Trail Canyon did not have an equivalent narrow thalweg. Instead, spring discharge diffusively covered a small portion of the channel bed with surface water in some places. In the discussion section we interpret how differences in grain size distribution (GSD) may influence channel morphology and the spatial distribution of vegetation on the bed and/or banks.

5.3 LiDAR and Anuga Flood Modeling

Figure 2 shows a modeled 30 m^3/s flood in a sparsely-vegetated reach and a densely-vegetated reach of Lower Woodruff Canyon. The sparsely-vegetated reach has a clearly-defined alluvial channel and floodplain inset into the bedrock canyon, with small amounts of vegetation on the channel margins and floodplain (Figure 2a, b). In contrast, the LiDAR shows that the densely-vegetated reach has multiple low-relief channel threads, and vegetation across the entire channel width (Figure 2h, i). In the sparsely-vegetated reach, there is a single thread of relatively high flow velocity (Figure 2c,d). In the densely-vegetated reach the active channel is significantly wider and average flow velocities are lower (Figure 2j, k).

In Trail Canyon, Figure 3 shows that the average flow velocity is higher and the channel is wider in the sparsely-vegetated reach compared to the densely-vegetated reach. Vegetation in Trail Canyon is preferentially located on the banks rather than the bed (Figure 3e), in contrast to Woodruff Canyon.

Figures 4, 5 and 6 show that channel slope is fairly constant through Upper and Lower Woodruff Canyon and Trail Canyon reaches in spite of large changes in vegetation density and width. The figures also demonstrate how width, depth, and velocity vary at our minimum and maximum modeled discharges of 10 and 50 m^3/s. Table 1 summarizes channel and flow characteristics from flood modeling. Along Trail Canyon, two narrow channel reaches are bounded on both sides by bedrock rather than alluvium; these are further described by Ouimet et al. (2008) and excluded from further analysis (Figure 6).

The impacts of variable roughness on width, depth, and flow velocity were minor relative to the influence of local topography along the channel (Figures 2-6), suggesting that hydraulic roughness may not be the dominant mechanism by which vegetation impacts channel morphology. Consistent with expectations, spatially variable roughness ($n > 0.04$) led to higher width and depth and lower flow velocity relative to constant roughness ($n = 0.04$). Spatially-variable Manning's n increased systematically with *LVI* (Figure 7). The only vegetation constraint used to calculate n is a measure of average canopy height (V_{ch}) from the LiDAR point cloud, not *LVI* directly (Equations 1-3). In our analysis n increases with discharge, even though flow depth is also increasing. In contrast, n is sometimes assumed to decrease with increasing discharge, as the ratio of flow depth relative to grain size increases and relative roughness decreases (e.g., Ferguson, 2007). However, we find that lower discharge flows tend to be more confined to less vegetated thalwegs. As discharge increases and the wetted width increases, the amount of flow interacting with hydraulically rough vegetation increases.

Figure 8 shows how channel width, hydraulic radius, and flow velocity vary with vegetation density and discharge for uniform roughness (n = 0.04) models. Correlations are quantified using the non-parametric Kendall rank correlation coefficient (τ) and associated p-values. For visual clarity, points have been binned into *LVI* increments of 0.1, although statistical calculations were performed using unbinned data for all discharges. Variable hydraulic roughness models have comparable correlations (Table 2). In general, width is most strongly and consistently correlated with vegetation density across the range of discharges. Width increases overall with *LVI* for both Woodruff springs but decreases for Trail. Depth and velocity tend to be weakly but significantly correlated with *LVI* at lower discharges, and weakly to insignificantly correlated at higher discharges. Hydraulic radius tends to decrease with increasing vegetation density for Woodruff, but increases for Trail Canyon. Even though *LVI* strongly correlates with n in the variable roughness case (Figure 7), the strengths and significance of correlations between *LVI*, channel morphology and flow velocity are quite similar for the uniform roughness and variable roughness cases. In addition, Table 2 Kendall τ values for uniform roughness are significantly correlated with τ for variable roughness (R^2=0.83, p≈0). This again suggests that the direct effects of vegetation on hydraulic roughness and flow are less important than the influence of vegetation on the underlying channel morphology.

5.4 Hydraulic geometry with sparse and dense vegetation

To further quantify how the distribution of vegetation on the bed and/or banks influences hydraulic geometry, we next classify channels into low-*LVI* and high-*LVI* cross sections. Based on field interpretations of sparse and dense vegetation, we use the criteria *LVI* < 0.1 as sparsely vegetated and *LVI* > 0.2 as densely vegetated for both Lower Woodruff and Upper Woodruff, where vegetation tends to cover both bed and banks (*B&BV*). In contrast, in Trail Canyon we use *LVI* < 0.075 and *LVI* > 0.1 to define sparsely and densely vegetated cross sections, respectively. These lower thresholds are consistent with lower overall *LVI* and predominantly bank-only vegetation (*BOV*). We then group width, depth, and velocity from sparsely and densely vegetated reaches into separate distributions (Supporting information Figures S1, S2).

Leopold and Maddock (1953) found that systematic variations in channel width, depth, and flow velocity as a function of discharge were well described by power laws:

$$W = a_w Q^{b_w} \quad (4)$$

$$D = a_d Q^{b_d} \quad (5)$$

$$V = a_v Q^{b_v} \quad (6)$$

Leopold and Maddock (1953) found b_w=0.26, b_d=0.4, b_v=0.34 when determined for different discharges at a particular river cross section, known as "at-a-station" hydraulic geometry. These exponents represent average values "representing a large variety of rivers in the Great Plains and the Southwest" [USA], and may be "biased towards semiarid conditions" (Leopold and Maddock, 1953). "Downstream" hydraulic geometry can also be evaluated by comparing channel dimensions and flow velocity at significantly different downstream locations that have different mean annual discharges (as also evaluated by Leopold and Maddock, 1953) or bankfull flood discharges. Leopold and Maddock (1953) report average exponents for downstream hydraulic geometry of b_w=0.5, b_d=0.4, b_v=0.1. While Huang and Nanson (1997) constrained downstream hydraulic geometry, our evaluation of channel morphology at different discharges represents at-a-station constraints.

Figure 9 shows best-fit regression lines to equations (4)-(6) for channel data classified as sparsely- and densely-vegetated. When the sparsely- and densely-vegetated fits are averaged over all channels for the uniform roughness case, overall $b_w = 0.30 \pm 0.04$ (± 1 standard error), consistent with b_w= 0.26 from Leopold and Maddock (1953). Similarly, we find b_d=0.42 ± 0.01 (close to b_d=0.4), and b_v= 0.28± 0.02 (relatively close to b_v= 0.34). Variable roughness exponents are similar ($b_w = 0.31 \pm 0.05$; b_d=0.44 ± 0.01; b_v=0.24± 0.02). Thus, our method provides at-a-station hydraulic geometry exponents that are reasonably consistent with previous work.

Channel width varies more between sparsely- and densely-vegetated reaches than do hydraulic radius and flow velocity (Figure 9). In Upper and Lower Woodruff Canyon, densely-vegetated reaches are wider, and to a lesser degree shallower with slower velocities. In Trail Canyon, densely-vegetated reaches are narrower and deeper, while velocities are largely unchanged. Again, differences between flow calculations using uniform n = 0.04 and vegetation-dependent n

were minor. In general, the addition of parameterized roughness did not significantly affect the exponents (b values) for hydraulic geometry relations, or how width, depth, or slope varied with increasing discharge between sparsely- and densely-vegetated reaches.

Finally, Figure 9j-l presents new regressions of downstream hydraulic geometry to data from Huang and Nanson (1997). The mean annual precipitation in their field area varied between 110 and 160 cm/yr (Huang and Nanson, 1997), more than 10x higher than our field site. They surveyed 30 total channel cross sections along four different channels, and calculated discharge based on their interpretations of bankfull conditions. They separately classified these data in terms of bed grain size (16 dominantly gravel-bed cross sections; 14 dominantly sand-bed cross sections) and vegetation (following names from Huang and Nanson (1997), six "no vegetation" cross sections, all in gravel; 18 "vegetation well down banks" cross sections, six "vegetation on both channel bed and banks" cross sections). We refer to their vegetation classes as NV (no vegetation), BOV (bank-only vegetation), and B&BV (bed and bank vegetation), respectively. The land directly adjacent to their channels has been cleared of larger vegetation and is actively used as pastureland (Huang and Nanson, 1997). Google Earth imagery suggests that their "no vegetation" reaches may have some cover by grasses and smaller vegetation, but no trees. Previous work demonstrates that grasses and similar vegetation can also be effective at stabilizing river banks (e.g., Micheli and Kirchner, 2002a,b).

Huang and Nanson (1997) calculated scaling factors a_w, a_d, a_v based on imposed downstream hydraulic geometry exponents of b_w=0.5, b_d=0.3, b_v=0.2 (similar to downstream b_w=0.5, b_d=0.4, b_v=0.1 found by Leopold and Maddock, 1953). For Figure 9j-l we use their vegetation classifications (NV, BOV, B&BV), regardless of grain size (sand-bed or gravel-bed). Our regressions to their data give average downstream b_w=0.43+-0.06 (±1 standard error), b_d=0.21±0.06, and b_v=0.33±0.08 (Figure 9j-l). At lower discharges, Huang and Nanson (1997) channels with B&BV are roughly double the width of the NV channels (Figure 9j). The relative difference in width decreases modestly with increasing discharge. This is consistent with our results comparing sparsely- and densely-vegetated reaches for Upper and Lower Woodruff Canyons (Figures 9a,b). Widths for their NV and BOV cases are also similar to our sparsely- and densely-vegetated Trail Canyon reaches (Figure 9c). Depth and velocity are more variable and show bigger differences among the channel classes than we found, but trends remain broadly consistent between our data and theirs.

5. Discussion

Our results show that vegetation density exerts a statistically-significant control on channel morphology, but the distribution of vegetation can drive channel width and/or depth in opposite directions. Most previous work has found that the effect of riparian vegetation is to narrow and deepen channels (e.g., Erskine et al., 2012; Friedman et al., 1996; Graf, 1978; Manners et al., 2014; Perignon et al., 2013; Tal and Paola, 2007). This is because much of the research on riparian vegetation and channel morphology has been focused on perennial streams with bank-only vegetation, where baseflow prevents establishment of stable plants on the bed. Our data quantify how riparian vegetation can also have the opposite effect and cause channel widening, consistent with the field analysis of Huang and Nanson (1997). After summarizing our data, we discuss how not only water availability but also grain size may control the distributions of bed vs bank vegetation in our particular field site, and interpret feedbacks that lead to both channel narrowing and widening in response to riparian vegetation.

Figure 10 synthesizes the quantitative differences between our densely- and sparsely-vegetated reaches as a function of discharge. At the lowest modeled discharge (10 m^3/s), Upper and Lower Woodruff channel cross sections with dense vegetation are ≈ 75-100% wider than sparsely-vegetated reaches. The difference in width decreases with discharge; at the highest modeled discharge (50 m^3/s), vegetated channel wetted widths are ≈ 20-50% wider than sparsely-vegetated channel widths. In contrast, densely-vegetated reaches in Trail Canyon are ≈ 25% narrower than sparsely-vegetated Trail reaches, a ratio that does not significantly vary with discharge. The responses of channel depth and flow velocity to vegetation are more variable along Woodruff Canyon (Figure 10b, c). Upper Woodruff's densely-vegetated reaches are ≈ 0-20% shallower than sparsely-vegetated reaches, while densely- and sparsely-vegetated Lower Woodruff reaches have roughly similar depths at similar discharges (≈0-10% different). In contrast, Trail canyon's densely-vegetated reaches are ≈15-20% deeper than sparsely-vegetated reaches. Cross-section averaged flow velocity has minimal sensitivity to vegetation for Trail Canyon velocities. Woodruff Canyon velocities are modestly slower in densely- compared to sparsely-vegetated reaches.

A key question is why the vegetation is distributed differently at the Trail Canyon spring compared to the Woodruff springs. Persistent water availability provided by subsurface springs is clearly a requirement for dense vegetation in this landscape. Perhaps differences in the amount or distribution of spring-supplied water play a role, although we do not have data constraining subsurface spring discharge through the reaches. It is also possible that light availability, influenced by canyon orientation, width and height plays a role (e.g., Julian et al., 2008). However, we think the most likely explanation is grain size. Trail Canyon sediment is much coarser overall than Woodruff, especially on the river bed. We interpret that even when vegetation does germinate on the channel bed of Trail, the coarse gravel in the root-zone makes it more difficult for the vegetation to become stabilized enough to withstand the next bedload-transporting flood. Vegetation has a more difficult time colonizing and stabilizing gravel bed surfaces compared to sand- and clay-rich river bars (e.g., Andreoli et al., 2020; Huang and Nanson, 1997 Karrenberg et al., 2003). Field observations of damage to tree trunk surfaces oriented upstream in the flow also attest to near-bed impacts from energetic coarse bedload transport that could likely obliterate young growth. In contrast, the channel banks and vegetated near-channel floodplain along Trail tend to be capped with sand and finer sediment deposited at higher flows. The vegetated bank tops flood more rarely than the bed, giving plants of all species more time to establish. Finer sediment on and near the bank tops may also cause water to be more consistently available for near-surface germination and growth due capillary rise from the subsurface and enhanced retention. Our qualitative field observations indicate that most gravels forming the Trail Canyon bed are clast-supported, which will be well-drained and will likely not hold as much near-surface water in their pores. Huang and Nanson (1997) similarly interpreted that grain size differences among channel reaches significantly influenced the distribution of vegetation. Their “no-vegetation” classification contains only gravel-bed cross sections, while their bed and bank vegetation (*B&BV*) classification only contains sand-bed cross sections.

The sediment along Woodruff Canyon is finer than along Trail, which likely facilitates channel bed seed germination in spring reaches. Along these spring reaches, we observe that both the bed and bank tend to consist of densely interlocked vegetation growing in thin soils. While we do not have grain size data to compare vegetated and non-vegetated reaches, we interpret that positive feedbacks between vegetation growth and enhanced trapping of fine sediment, including cohesive clays, may also promote vegetation growth in Woodruff spring reaches. During smaller floods, the abundant bed vegetation slows down near-bed flow, enhancing deposition of fine sediment on the bed, which may further stabilize existing vegetation and add clay cohesion. More vegetation also creates and traps more leaf litter, which may further enhance both cohesive soil development and nutrient availability on the channel bed and banks.

"Threshold channels" provide a useful conceptual framework in which to interpret how vegetation may impact width, depth, and velocity. In this theory, channel morphology adjusts such that the threshold for erosion or entrainment is just barely exceeded everywhere along the cross-section boundary. It was originally developed for non-cohesive gravel-bed channels in which thresholds of grain motion can be well constrained (Parker, 1978). Recent work has also shown that threshold erodibility applies much more broadly to channel adjustment when banks are clay-rich and cohesive, as is typical for many rivers with both sand and gravel beds (Dunne and Jerolmack, 2020).

In the sparsely-vegetated reaches of both Woodruff and Trail Canyons, the vegetation is preferentially found on channel banks, which adds bank strength. Interestingly, Figure 9 indicates that the width scaling of sparsely-vegetated Woodruff and Trail reaches is similar in spite of grain size differences. We interpret that bank vegetation rather than grain size may set the "threshold" for channel width in the sparsely-vegetated reaches of these channels. For Trail Canyon, the densely-vegetated reach is ≈25% narrower and deeper than the sparsely-vegetated reach (Figure 10). This is qualitatively consistent with threshold channel expectations because increasing bank strength (by increasing vegetation density) while keeping bed strength the same (noncohesive gravel) should lead to narrower and deeper channels.

For the densely-vegetated Upper and Lower Woodruff reaches, relative to the sparsely-vegetated reaches, we interpret that the increase in *bed* vegetation (from essentially no vegetation to dense cover) increases bed strength more than the increase in bank vegetation (from some vegetation to dense cover) increases bank strength, resulting in widening and shallowing. Huang and Nanson (1997) hypothesize that hydraulic roughness and flow constrictions from vegetation may divert more higher-velocity flow into channel banks, enhancing bank erosion and widening. Modeling by Bywater-Reyes et al. (2018) supports this feedback. Woody vegetation may enhance near-bank turbulence and shear stresses more than grasses (McBride et al., 2007). Bed deposition enhanced by dense near-bed vegetation (e.g., Luhar et al., 2008) could also cause shallowing and widening. In Woodruff spring reaches, if channel bed vegetation captured more sediment than did bank vegetation, then the channel would become shallower. For a given flood discharge (and reach slope and average velocity), a shallower flow will result in a wider wetted width. The longitudinal channel profiles (Figures 4a, 5a, 6a) indicate that reach slope minimally adjusts to changes in vegetation in these channels, suggesting that width, depth, and bed topography coevolve in response to vegetation. Various combinations of local erosion and/or deposition could lead to similar channel adjustments due to strength and roughness effects of vegetation.

Future work could mechanistically explore how vegetation and hydrological properties result in the morphological differences observed in our LiDAR and flow modeling analysis. We assumed that the effects of vegetation on flow can be accounted for through spatially variable hydraulic roughness, rather than direct effects of vegetation obstructing local flow. We lack good constraints on the flood recurrence intervals corresponding to the modeled discharges, although the 10-50 m^3/s discharges include both flows contained within the channels as well as overbank flows. The hydraulic geometry approach assumes that the same power-law scaling holds over a broad range of discharges, and so the at-a-station exponents quantified here ought to be insensitive to exactly the discharges used. We do not have direct constraints on bulk bank or bed strength and how it varies with LVI. Field data collection could quantify variables that may be more influential than simple vegetation density and relate them back to the analysis presented here, including bed and bank strength, root characteristics, the spatial distributions of plant species, nutrient availability, soil cohesion, and grain size distributions. Soil moisture and streamflow monitoring would be useful for characterizing seasonal water availability and flood recurrence intervals. Monitoring solar radiation, temperature, humidity, and precipitation in different reaches could likewise be informative for understanding how spring and flood water availability influence riparian vegetation and feedbacks with channel and floodplain form.

6. Conclusions

The pervasiveness of vegetation at Earth’s surface, its tendency to vary with regional climate, and the complexity of hydrologic and substrate feedbacks that influence channel morphology all make it challenging to isolate controls of vegetation on river channel morphology. Our study demonstrates that vegetation feedbacks established in perennially flowing channels may not apply to intermittently flowing channels. Localized groundwater springs at our dryland study reaches lead to large changes in vegetation density over short distances. This allowed us to better isolate vegetation impacts by controlling for flood discharge and long-term sediment supply, which must be the same despite variable vegetation density.

Channel geometry varies with both the amount and spatial distribution of vegetation in and along channels. Channel width is more sensitive to vegetation changes than is depth or flow velocity. Vegetation can have opposite effects on width: dense vegetation on the channel bed correlates with wider and shallower channels (Upper and Lower Woodruff Canyon), while dense vegetation focused on channel banks causes narrower and deeper reaches (Trail Canyon). We interpret that the difference in vegetation distribution between Woodruff and Trail Canyons was likely caused by grain size differences: Trail Canyon has a much coarser channel bed, which inhibited the establishment of stable and resilient bed vegetation in spite of only having intermittent flow. These results are generally consistent with findings of Huang and Nanson (1997).

The effects of spatially uniform versus spatially variable and vegetation-dependent hydraulic roughness on modeled flow width, depth, and velocity were surprisingly small. This suggests that the underlying bed and bank topography of channels (which coevolves with vegetation) may have a larger effect on flow than the vegetation itself. Simply assuming a spatially uniform hydraulic roughness may be sufficient for some flood modeling applications using high resolution bed topography. While width, depth, and velocity vary systematically with vegetation density, power-law scaling exponents describing how these variables vary with discharge (i.e., at-a-station hydraulic geometry) are consistent with previous work (e.g. Leopold and Maddock, 1953; Huang and Nanson, 1997). Perhaps this should not be surprising, as the subtle but pervasive effects of vegetation are implicit in essentially all analyses of terrestrial river channels.

Data Availability Statement

Flow modeling data used in our analyses are available in tables in Supporting information, and will also be made publicly available as a data archive that meets AGU requirements through the

Texas Data Repository (data.tdl.org) if the manuscript is accepted. LiDAR data are available at https://doi.org/10.5069/G9NC5Z4W.

Acknowledgements

This paper is based on the Master's Thesis of Southard (2019). The work was funded by The University of Texas at Austin Jackson School of Geosciences and a Geological Society of America Student Research Grant. All authors contributed to project design. PS and JPLJ wrote the manuscript, with input from DR and AMM. We thank C.L. McCafferty, Joshua Pikovsky and Wayne Baumgartner for field assistance, and the National Center for Airborne Laser Mapping (NCALM) and Lindsay Olinde for the airborne LiDAR data.

Figure Captions

Figure 1: a. Henry Mountains, Utah regional map, showing elevations of LiDAR coverage with Trail Canyon (spring located at ≈37.8879 N, 110.5306 W), Upper Woodruff (spring located at ≈37.8637 N, 110.5872 W), and Lower Woodruff Canyon (spring located at ≈37.8645 N, 110.5484 W). Two bedrock reaches ("Br reaches") along Trail Canyon were excluded from the analysis. b, c. Woodruff channel, upstream and downstream of lower spring, respectively. d, e. Woodruff channel, upstream and downstream of upper spring, respectively. f, g. Trail Canyon channel, upstream and downstream of spring. h. View from above very narrow thalweg at upper Woodruff spring; perennial spring discharge maintains a vegetation-free width of ≈15-20 cm. Grass adjacent to thalweg had been knocked down by recent flooding. i. Trail canyon bedrock sidewall, showing groundwater seepage and minor "hanging gardens" in vicinity of spring.

Figure 2: Lower Woodruff Canyon, 30 m^3/s modeled discharge. The bottom two maps show LiDAR elevations and locations of smaller maps with sparse vegetation upstream (a-g) and denser vegetation downstream (h-n), as well as LVI (bottom left) and depth-averaged velocity (bottom right). Grid numbers are UTM Zone 12 N coordinates. The east-west spacing between the vertical grid lines is 1 km. Panels a-n are 250 m wide. a,h: Shaded relief of LiDAR topography gridded to 1 m. b,i: Lidar Vegetation Index (LVI). c,j: Velocity, uniform roughness (n=0.04). d,k: Velocity, variable hydraulic roughness. e,l: Spatially variable (vegetation-

dependent) Manning's n. f,m: Flow depth, uniform roughness. g,n: Flow depth, variable roughness.

Figure 3: Trail Canyon, 30 m^3/s modeled discharge. Description of figure panels is otherwise the same as for Figure 2.

Figure 4: Lower Woodruff Canyon. a. Longitudinal channel profile indicates relatively little reach slope change with LiDAR Vegetation Index (LVI; gray, right-hand y axis). b. Manning's n, showing uniform roughness (n=0.04), and spatially variable Manning's n calculated at discharges of 10 and 50 m^3/s. c,d,e. Wetted width, hydraulic radius, and velocity, respectively, at 10 and 50 m^3/s, for uniform and variable Manning's n. "Downstream Distance" starts at an arbitrary position along the channel.

Figure 5: Upper Woodruff Canyon. Description of figure panels is otherwise the same as for Figure 4.

Figure 6: Trail Canyon. Bedrock reaches excluded from subsequent analyses represent narrow epigenetic gorge reaches where width appears controlled by bedrock walls and more recent bedrock incision (Ouimet et al., 2008), rather than being able to adjust by eroding alluvium. Description of figure panels is otherwise the same as for Figure 4.

Figure 7: When calculated for the variable roughness case, Manning's n increases with LVI and also with discharge. Crosses represent averaged Manning's n for bins spanning 0.1 LVI, with their size indicating that bin's proportion of the overall dataset. For visual clarity, 20 and 40 m^3/s discharges are not shown. Dashed lines represent linear regressions.

Figure 8: Correlations between LiDAR Vegetation Index and wetted width, hydraulic radius, and cross-section averaged velocity, at discharges of 10, 30, and 50 m^3/s, for uniform roughness models (n=0.04). Data are binned in LVI increments of 0.1 (0-0.1, 0.1-0.2, etc.). Data for 10 and 50 m^3/s are offset from the LVI bin centers (0.05, 0.15, etc.) for visual clarity. Whiskers span ±1 standard deviation. Size of points represents the relative proportion of data points in that bin. Legends show Kendall τ coefficient and associated p-values; statistically significant correlations ($p<0.05$) are highlighted in red.

Figure 9a-i: Best-fit hydraulic geometry scaling for uniform hydraulic roughness and spatially variable hydraulic roughness, for data classified as sparsely- and densely-vegetated. The panel d legend (i.e, sparse and dense vegetation, uniform and variable n) applies to panels a-i. Data points are not shown in order to better visualize the relations among fits. Additional bounding lines visually indicate 95% confidence intervals on regression parameters (coefficient and exponent) for the variable roughness cases; uncertainties are similar for uniform roughness regressions. j-l. Huang and Nanson (1997) data and our regressions to them. Note that k reflects depth, while d,e,f reflect hydraulic radius.

Figure 10: Percent change between sparsely- and densely-vegetated reaches in terms of channel (a) width, (b) hydraulic radius, and (c) flow velocity, over the range of discharges modeled in this study. Percent change was calculated from the regression curves shown in Figure 9, as the densely-vegetated curve minus the sparsely-vegetated curve divided by the sparsely-vegetated curve. Positive % change values (green arrow) indicate that the densely-vegetated case is larger that the sparsely-vegetated case. Negative values (red curve) indicate that the sparsely-vegetated case is larger. Along Trail canyon, for example, densely-vegetated reaches are ≈25% narrower than sparsely-vegetated reaches, and this difference is relatively insensitive to discharge. In contrast, for both Woodruff spring reaches, densely-vegetated widths are nearly double sparsely vegetated widths at low discharges. At higher discharges, densely-vegetated widths are ≈20 to 40% higher than sparsely-vegetated widths. Channel width (a) is more sensitive to vegetation than are hydraulic radius (b) or flow velocity (c).

Works Cited

Abu-Aly, T. R., Pasternack, G. B., Wyrick, J. R., Barker, R., Massa, D., & Johnson, T. (2014). Effects of LiDAR-derived, spatially distributed vegetation roughness on two-dimensional hydraulics in a gravel-cobble river at flows of 0.2 to 20 times bankfull. Geomorphology, 206, 468-482. https://doi.org/10.1016/j.geomorph.2013.10.017

Andreoli, A., Chiaradia, E. A., Cislaghi, A., Bischetti, G. B., & Comiti, F. (2020). Roots reinforcement by riparian trees in restored rivers. Geomorphology, 370, 107389. https://doi.org/10.1016/j.geomorph.2020.107389

Arcement, G. J., & Schneider, V. R. (1989). Guide for selecting Manning's roughness coeffcients for natural channels and flood plains (USGS Numbered Series No. 2339).

Barnes, H. (1967). Roughness characteristics of natural channels. United States Geological Survey Water Supply Paper 1849.

Braudrick, C. A., Dietrich, W. E., Leverich, G. T., Sklar, L. S. (2009). Experimental evidence for the conditions necessary to sustain meandering in coarse-bedded rivers. Proceedings of the National Academy of Sciences, 106 (40) 16936-16941. https://doi.org/10.1073/pnas.0909417106

Bywater-Reyes, S., Diehl, R. M., and Wilcox, A. C. (2018). The influence of a vegetated bar on channel-bend flow dynamics, Earth Surf. Dynam., 6, 487–503, https://doi.org/10.5194/esurf-6-487-2018

Bywater-Reyes, S., Wilcox, A. C., and Diehl, R. M. (2017), Multiscale influence of woody riparian vegetation on fluvial topography quantified with ground-based and airborne lidar, *J. Geophys. Res. Earth Surf.*, 122, 1218– 1235, https://doi.org/10.1002/2016JF004058

Camporeale, C., Perucca, E., Ridol_, L., & Gurnell, A. M. (2013). Modeling the Interactions Between River Morphodynamics and Riparian Vegetation. Reviews of Geophysics, 51 (3), https://doi.org/10.1002/rog.20014

Casas, A., Lane, S. N., Yu, D., & Benito, G. (2010). A method for parameterizing roughness and topographic sub-grid scale effects in hydraulic modelling from LiDAR data. Hydrol. Earth Syst. Sci., 14, 1567–1579, https://doi.org/10.5194/hess-14-1567-2010

Coulthard, T. J. (2005). Effects of vegetation on braided stream pattern and dynamics. Water Resources Research, 41 (4). https://doi.org/10.1029/2004WR003201

Corenblit, D., & Steiger, J. (2009). Vegetation as a major conductor of geomorphic changes on the Earth surface: toward evolutionary geomorphology. Earth Surface Processes and Landforms, 34 (6), 891-896. https://doi.org/10.1002/esp.1788

Corenblit, D., Tabacchi, E., Steiger, J., & Gurnell, A. M. (2007). Reciprocal interactions and adjustments between fluvial landforms and vegetation dynamics in river corridors: A review of complementary approaches. Earth-Science Reviews, 84 (1), 56-86. https://doi.org/10.1016/j.earscirev.2007.05.004

Crosato, A., & Saleh, M. S. (2011). Numerical study on the effects of floodplain vegetation on river planform style. Earth Surface Processes and Landforms, 36 (6), 711-720. https://doi.org/10.1002/esp.2088

Dean, D.J. and Topping, D.J. (2019). Geomorphic change and biogeomorphic feedbacks in a dryland river: The Little Colorado River, Arizona, USA. GSA Bulletin, *131*(11-12), pp.1920-1942. https://doi.org/10.1130/B35047.1

Dunkerley, D. L. (1992). Channel geometry, bed material, and inferred flow conditions in ephemeral stream systems, barrier range, western N.S.W. Australia. Hydrological Processes, 6 (4), 417-433. https://doi.org/10.1002/hyp.3360060404

Dunne, K. B. J., & Jerolmack, D. J. (2020). What sets river width? Science Advances, 6(41), eabc1505. https://doi.org/10.1126/sciadv.abc1505

Erskine, W., Keene, A., Bush, R., Cheetham, M., & Chalmers, A. (2012). Influence of riparian vegetation on channel widening and subsequent contraction on a sand-bed stream since European settlement: Widden Brook, Australia. Geomorphology, 147-148, 102-114. https://doi.org/10.1016/j.geomorph.2011.07.030

Ferguson, R. (2007), Flow resistance equations for gravel- and boulder-bed streams, Water Resour. Res., 43, W05427, https://doi.org/10.1029/2006WR005422

Fischenich, J. C. (1997). Hydraulic Impacts of Riparian Vegetation; Summary of the Literature (Tech. Rep. EL-97-9). Environmental Impact Research Program, U.S. Army Corps of Engineers.

Friedman, J. M., Osterkamp, W. R., & Lewis, W. M. (1996). Channel Narrowing and Vegetation Development Following a Great Plains Flood. Ecology, 77 (7), 2167-2181. https://doi.org/10.2307/2265710

Gilbert, G. K. (1877). Geology of the Henry Mountains. U.S. Geographical and Geological Survey of the Rocky Mountains Region, Government Printing Office, Washington, D.C. https://doi.org/ 10.3133/70038096

González, E., Sher, A. A., Tabacchi, E., Masip, A., & Poulin, M. (2015). Restoration of riparian vegetation: A global review of implementation and evaluation approaches in the international, peer-reviewed literature. Journal of Environmental Management, 158, 85-94. https://doi.org/10.1016/j.jenvman.2015.04.033

Graf, W. L. (1978). Fluvial adjustments to the spread of tamarisk in the Colorado Plateau region. GSA Bulletin, 89 (10), 1491-1501. https://doi.org/10.1130/0016-7606(1978)89h1491:FATTSOi2.0.CO;2

Gran, K., & Paola, C. (2001). Riparian vegetation controls on braided stream dynamics. Water Resources Research, 37 (12), 3275-3283. https://doi.org/10.1029/2000WR000203

Gurnell, A. (2014). Plants as river system engineers. Earth Surf. Process. Landf. 39 (1), 4–25. https://doi.org/10.1002/esp.3397

Gurnell, A. M., Corenblit, D., García de Jalón, D., González del Tánago, M., Grabowski, R. C., O'Hare, M. T., and Szewczyk, M. (2016) A Conceptual Model of Vegetation–hydrogeomorphology Interactions Within River Corridors. *River Res. Applic.*, 32: 142– 163. https://doi.org/10.1002/rra.2928.

Hey, R. D., & Thorne, C. R. (1986). Stable Channels with Mobile Gravel Beds. Journal of Hydraulic Engineering, 112 (8), 671-689. https://doi.org/10.1061/(ASCE)0733-9429(1986)112:8(671)

Hickin, E. J. (1984). Vegetation and River Channel Dynamics. The Canadian Geographer / Le Geographe canadien, 28 (2), 111-126. https://doi.org/10.1111/j.1541-0064.1984.tb00779.x

Huang, H., & Nanson, G. C. (1997). Vegetation and channel variation; a case study of four small streams in southeastern Australia. Geomorphology, 18 (3-4), 237-249. https://doi.org/10.1016/S0169-555X(96)00028-1

Hunt, C. B., Averitt, P., & Miller, R. L. (1953). Geology and geography of the Henry Mountains region, Utah. Geological Survey Professional paper 228. https://doi.org/10.3133/pp228

Hupp, C. R., & Osterkamp, W. R. (1996). Riparian vegetation and fluvial geomorphic processes. Geomorphology, 14 (4), 277-295. https://doi.org/10.1016/0169-555X(95)00042-4

Johnson, J. P. L., Whipple, K. X., Sklar, L. S., & Hanks, T. C. (2009). Transport slopes, sediment cover, and bedrock channel incision in the Henry Mountains, Utah. Journal of Geophysical Research, 114 (F2). https://doi.org/10.1029/2007JF000862

Johnson, J. P. L., Whipple, K. X., Sklar, L. S. (2010). Contrasting bedrock incision rates from snowmelt and flash floods in the Henry Mountains, Utah. *GSA Bulletin*; September/October 2010; v. 122; no. 9/10; p. 1600–1615; https://doi.org/10.1130/B30126.1

Julian, J. P., Doyle, M. W., and Stanley, E. H. (2008), Empirical modeling of light availability in rivers, *J. Geophys. Res.*, 113, G03022, https://doi.org/10.1029/2007JG000601

Karrenberg, S., Blaser, S., Kollmann, J., Speck, T., & Edwards, P. J. (2003). Root Anchorage of Saplings and Cuttings of Woody Pioneer Species in a Riparian Environment. *Functional Ecology*, *17*(2), 170–177. http://www.jstor.org/stable/3599172

Katul, G., Wiberg, P., Albertson, J., & Hornberger, G. (2002). A mixing layer theory for flow resistance in shallow streams. Water Resources Research, 38 (11). https://doi.org/10.1029/2001WR000817

Kellerhals, R., & Bray, D. I. (1971). Sampling Procedures for Coarse Fluvial Sediments. Journal of the Hydraulics Division, 97(8), 1165-1180. https://doi.org/10.1061/JYCEAJ.0003044

Leopold, L. B., & Maddock, T. (1953). The hydraulic geometry of stream channels and some physiographic implications. U. S. Geological Survey Professional Paper 252. https://doi.org/10.3133/pp252

Luhar, M., Rominger, J. & Nepf, H. (2008). Interaction between flow, transport and vegetation spatial structure. *Environ Fluid Mech* **8,** 423. https://doi.org/10.1007/s10652-008-9080-9

Manners, R. B., Schmidt, J. C., & Scott, M. L. (2014). Mechanisms of vegetation-induced channel narrowing of an unregulated canyon river: Results from a natural field-scale experiment. Geomorphology, 211, 100-115. https://doi.org/10.1016/j.geomorph.2013.12.033

Manning, A., Julian, J.P. and Doyle, M.W. (2020). Riparian vegetation as an indicator of stream channel presence and connectivity in arid environments. *Journal of Arid Environments*, *178*. https://doi.org/10.1016/j.jaridenv.2020.104167

McBride, M., Hession, W.C., Rizzo, D.M. and Thompson, D.M. (2007), The influence of riparian vegetation on near-bank turbulence: a flume experiment. Earth Surf. Process. Landforms, 32: 2019-2037. https://doi.org/10.1002/esp.1513

Micheli, E. R., & Kirchner, J. W. (2002a). Effects of wet meadow riparian vegetation on streambank erosion. 1. Remote sensing measurements of streambank migration and erodibility. Earth Surface Processes and Landforms, 27(6), 627-639. https://doi.org/10.1002/esp.338

Micheli, E. R., & Kirchner, J. W. (2002b). Effects of wet meadow riparian vegetation on streambank erosion. 2. Measurements of vegetated bank strength and consequences for failure mechanics. Earth Surface Processes and Landforms, 27(7), 687-697. https://doi.org/10.1002/esp.340

Milan, D.J., Tooth, S. and Heritage, G.L. (2020). Topographic, hydraulic, and vegetative controls on bar and island development in mixed bedrock-alluvial, multichanneled, dryland rivers. *Water Resources Research*, *56*(5). https://doi.org/10.1029/2019WR026101

Millar, R. G. (2000). Influence of bank vegetation on alluvial channel patterns. Water Resources Research, 36 (4), 1109-1118. https://doi.org/10.1029/1999WR900346

Millennium Ecosystem Assessment, 2005. Ecosystems and Human Well-being: Desertification Synthesis. World Resources Institute, Washington, DC. ISBN 1-56973-590-5

Murray, A. B., & Paola, C. (2003). Modelling the effect of vegetation on channel pattern in bedload rivers. Earth Surface Processes and Landforms, 28 (2), 131-143. https://doi.org/10.1002/esp.428

Nepf, H. M. (1999). Drag, turbulence, and diffusion in flow through emergent vegetation. Water Resources Research, 35 (2), 479-489. https://doi.org/10.1029/1998WR900069

Olinde, LJ, 2012, Hite, UT: Quantifying Evolution and Stability of Coarse Alluvial Channels. National Center for Airborne Laser Mapping (NCALM), distributed by OpenTopography. https://doi.org/10.5069/G9NC5Z4W

Osterkamp, W. R., & Hupp, C. R. (2010). Fluvial processes and vegetation: Glimpses of the past, the present, and perhaps the future. Geomorphology, 116 (3), 274-285. https://doi.org/10.1016/j.geomorph.2009.11.018

Ouimet, W. B., K. X. Whipple, B. T. Crosby, J. P. Johnson, and T. F. Schildgen (2008), Epigenetic gorges in fluvial landscapes, Earth Surf. Processes Landforms, https://doi.org/10.1002/esp.1650.

Parker, G. (1978). Self-formed straight rivers with equilibrium banks and mobile bed. Part 2. The gravel river. *Journal of Fluid Mechanics, 89*(1), 127-146. https://doi.org/10.1017/S0022112078002505

Perignon, M. C., Tucker, G. E., Griffin, E. R., & Friedman, J. M. (2013). Effects of riparian vegetation on topographic change during a large flood event, Rio Puerco, New Mexico, USA.

Journal of Geophysical Research: Earth Surface, 118 (3), 1193-1209. https://doi.org/10.1002/jgrf.20073

Pietsch, T. J., & Nanson, G. C. (2011). Bankfull hydraulic geometry; the role of in-channel vegetation and downstream declining discharges in the anabranching and distributary channels of the Gwydir distributive fluvial system, southeastern Australia. Geomorphology, 129 (1), 152-165. https://doi.org/10.1016/j.geomorph.2011.01.021

PRISM Climate Group, 2021, Oregon State University, http://prism.oregonstate.edu, Monthly 1981-2010 Normals, created 15 September 2021.

Roberts, S., Nielsen, O., Gray, D., Sexton, J., & Davies, G. (2015). ANUGA User Manual, Release 2.0. https://doi.org/10.13140/RG.2.2.12401.99686

Simon, A., & Collison, A. J. C. (2002). Quantifying the mechanical and hydrologic effects of riparian vegetation on streambank stability. Earth Surface Processes and Landforms, 27 (5), 527-546. https://doi.org/10.1002/esp.325

Smith, D. G. (1976). Effect of vegetation on lateral migration of anastomosed channels of a glacier meltwater river. GSA Bulletin, 87 (6), 857-860. https://doi.org/10.1130/0016-7606(1976)87<857:EOVOLM>2.0.CO;2

Southard, P. J. (2019). Impact of spring-associated riparian vegetation on channel morphology: insights from Henry Mountains, UT. Master's Thesis, The University of Texas at Austin. https://doi.org/10.26153/tsw/2967

Tal, M., Gran, K., Murray, A. B., Paola, C., & Hicks, D. M. (2013). Riparian Vegetation as a Primary Control on Channel Characteristics in Multi-Thread Rivers. in Riparian Vegetation and Fluvial Geomorphology (pp. 43-58). American Geophysical Union (AGU). https://doi.org/10.1029/008WSA04

Tal, M., & Paola, C. (2007). Dynamic single-thread channels maintained by the interaction of flow and vegetation. Geology, 35 (4), 347. https://doi.org/10.1130/G23260A.1

Tal, M., & Paola, C. (2010). Effects of vegetation on channel morphodynamics: results and insights from laboratory experiments. Earth Surface Processes and Landforms, 35 (9), 1014-1028. https://doi.org/10.1002/esp.1908

Vargas-Luna, A., Crosato, A., Anders, N., Hoitink, A. J. F., Keesstra, S. D., & Uijttewaal, W. S. J. (2018). Morphodynamic effects of riparian vegetation growth after stream restoration. Earth Surface Processes and Landforms, 43 (8), 1591-1607. https://doi.org/10.1002/esp.4338

Wende, R., & Nanson, G. C. (1998). Anabranching rivers: ridge-form alluvial channels in tropical northern Australia. Geomorphology, 22 (3), 205-224. https://doi.org/10.1016/S0169-555X(97)00085-8

Wiel, M. J. V. D., & Darby, S. E. (2013). Numerical Modeling of Bed Topography and Bank Erosion Along Tree-Lined Meandering Rivers. in Riparian Vegetation and Fluvial

Geomorphology, S. J. Bennett & Andrew Simon, Eds., American Geophysical Union (AGU). pp. 267-282. https://doi.org/10.1029/008WSA19

Yager, E.M. and M.W. Schmeeckle, (2013). The influence of vegetation on turbulence and bedload transport, *JGR-Earth Surface*, 118, 1-17. https://doi.org/10.1002/jgrf.20085.

Figure 1

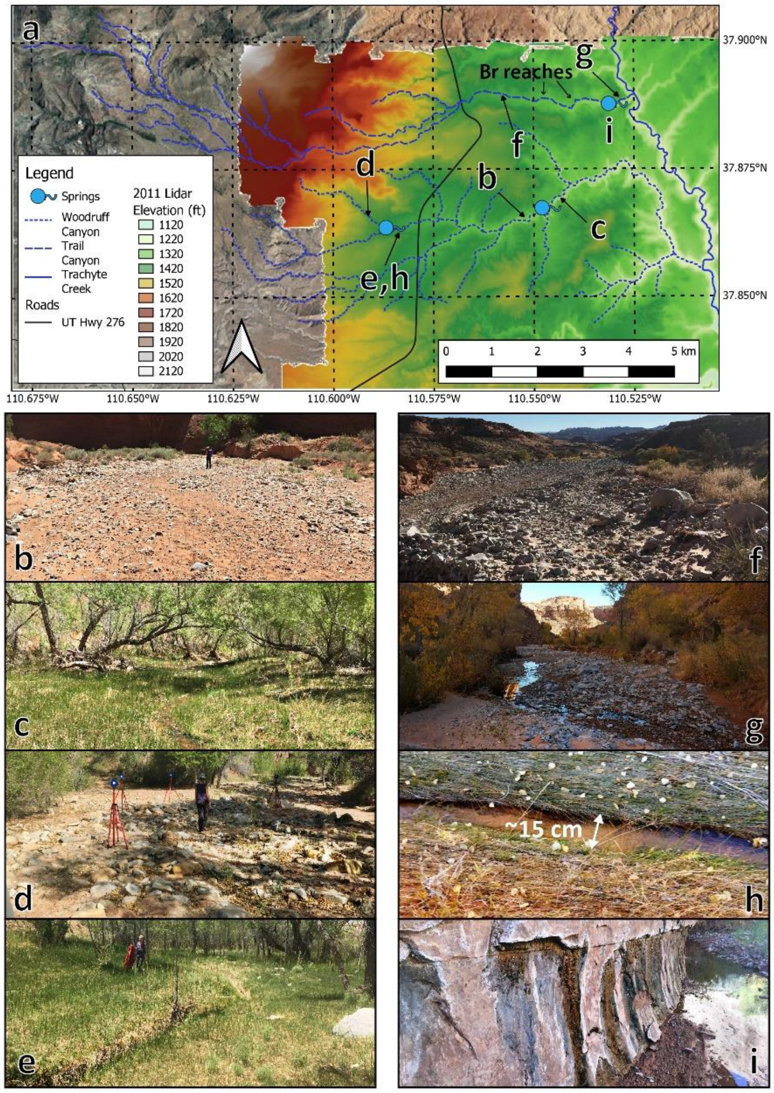

Figure 1: a. Henry Mountains, Utah regional map, showing elevations of LiDAR coverage with Trail Canyon (spring located at ≈37.8879 N, 110.5306 W), Upper Woodruff (spring located at ≈37.8637 N, 110.5872 W), and Lower Woodruff Canyon (spring located at ≈37.8645 N, 110.5484 W). Two bedrock reaches (“Br reaches”) along Trail Canyon were excluded from the analysis. b, c. Woodruff channel, upstream and downstream of lower spring, respectively. d, e. Woodruff channel, upstream and downstream of upper spring, respectively. f, g. Trail Canyon channel, upstream and downstream of spring. h. View from above very narrow thalweg at upper Woodruff spring; perennial spring discharge maintains a vegetation-free width of ≈15-20 cm. Grass adjacent to thalweg had been knocked down by recent flooding. i. Trail canyon bedrock sidewall, showing groundwater seepage and minor “hanging gardens” in vicinity of spring.

Figure 2

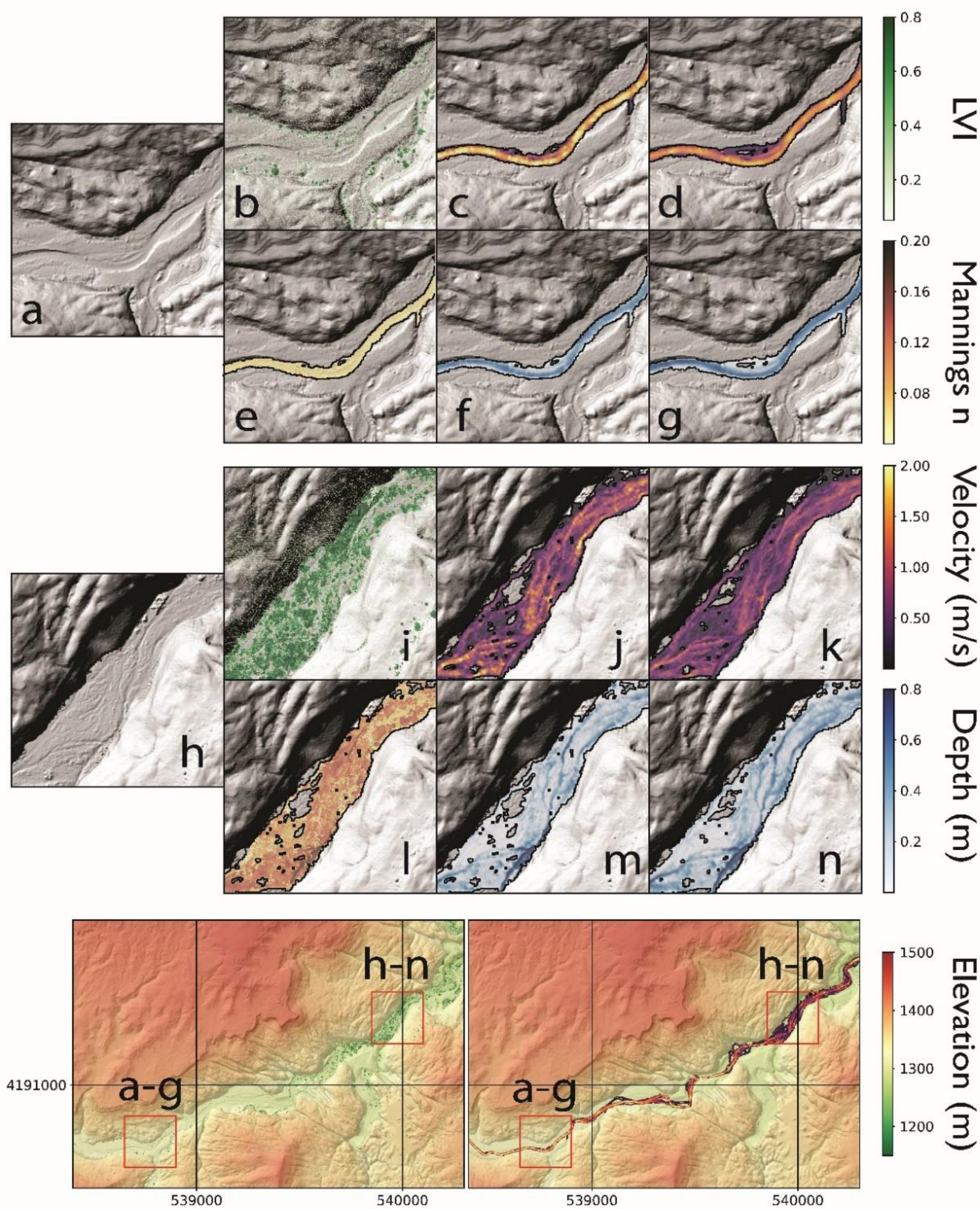

Figure 2: Lower Woodruff Canyon, 30 m^3/s modeled discharge. The bottom two maps show LiDAR elevations and locations of smaller maps with sparse vegetation upstream (a-g) and denser vegetation downstream (h-n), as well as LVI (bottom left) and depth-averaged velocity (bottom right). Grid numbers are UTM Zone 12 N coordinates. The east-west spacing between the vertical grid lines is 1 km. Panels a-n are 250 m wide. a,h: Shaded relief of LiDAR topography gridded to 1 m. b,i: Lidar Vegetation Index (LVI). c,j: Velocity, uniform roughness (n=0.04). d,k: Velocity, variable hydraulic roughness. e,l: Spatially variable (vegetation-dependent) Manning's n. f,m: Flow depth, uniform roughness. g,n: Flow depth, variable roughness.

Figure 3

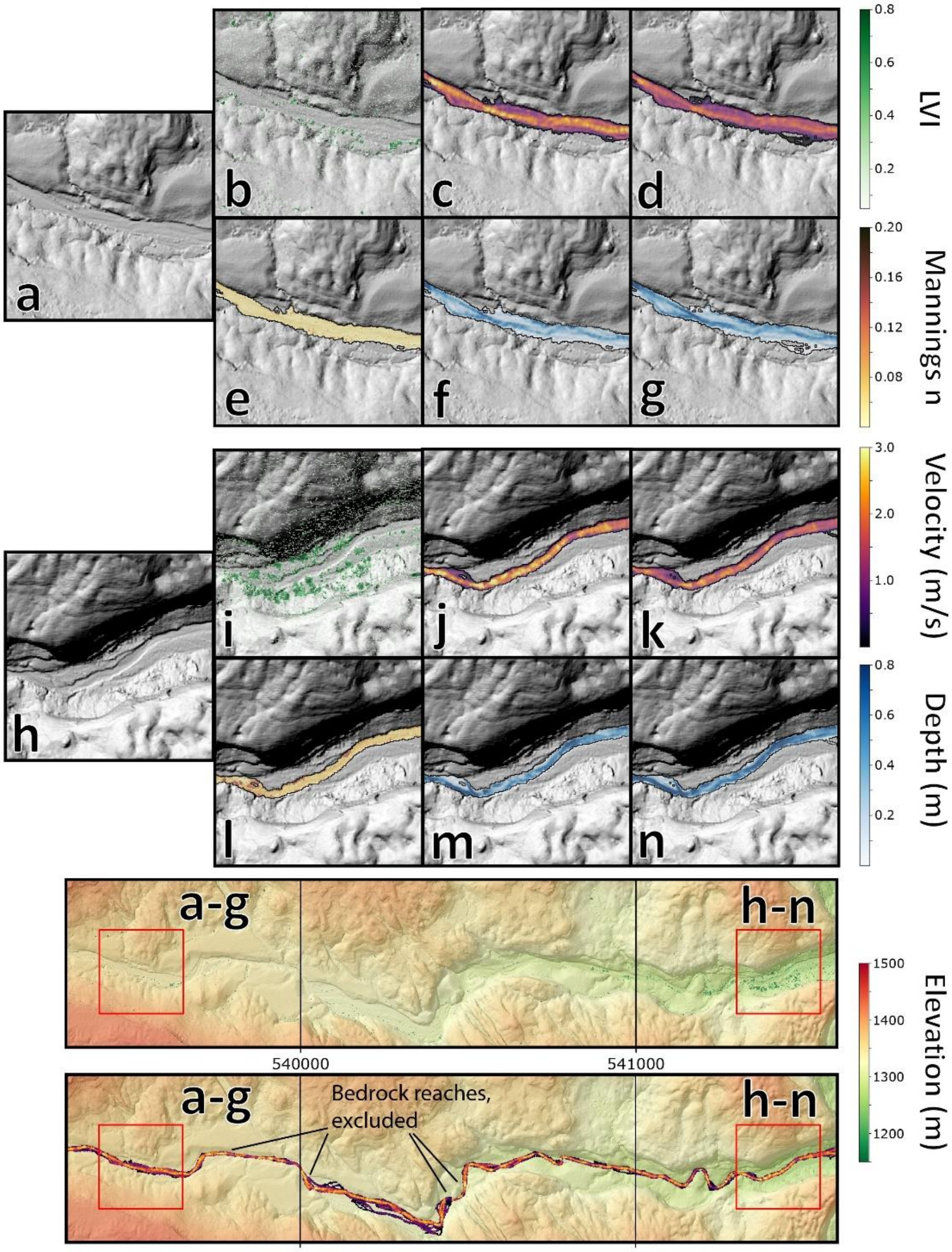

Figure 3: Trail Canyon, 30 m^3/s modeled discharge. Bottom map indicates extent (between sets of lines) of two bedrock-walled reaches excluded from subsequent analysis. Description of figure panels is otherwise the same as for Figure 2.

Figure 4

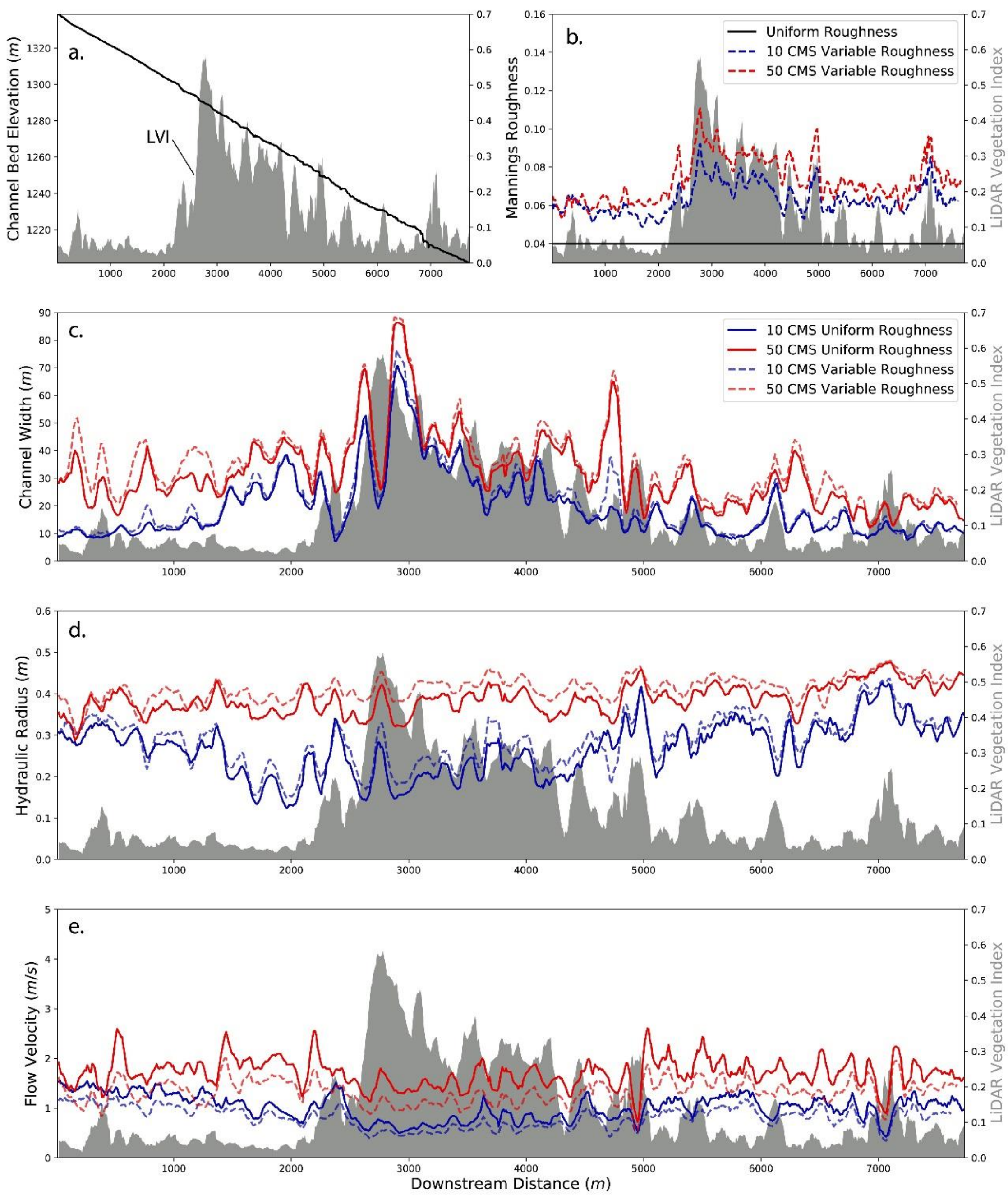

Figure 4: Lower Woodruff Canyon. a. Longitudinal channel profile indicates relatively little reach slope change with LiDAR Vegetation Index (LVI; gray, right-hand y axis). b. Manning's n, showing uniform roughness (n=0.04), and spatially variable Manning's n calculated at discharges of 10 and 50 m^3/s. c,d,e. Wetted width, hydraulic radius, and velocity, respectively, at 10 and 50 m^3/s, for uniform and variable Manning's n. "Downstream Distance" starts at an arbitrary position along the channel.

Figure 5

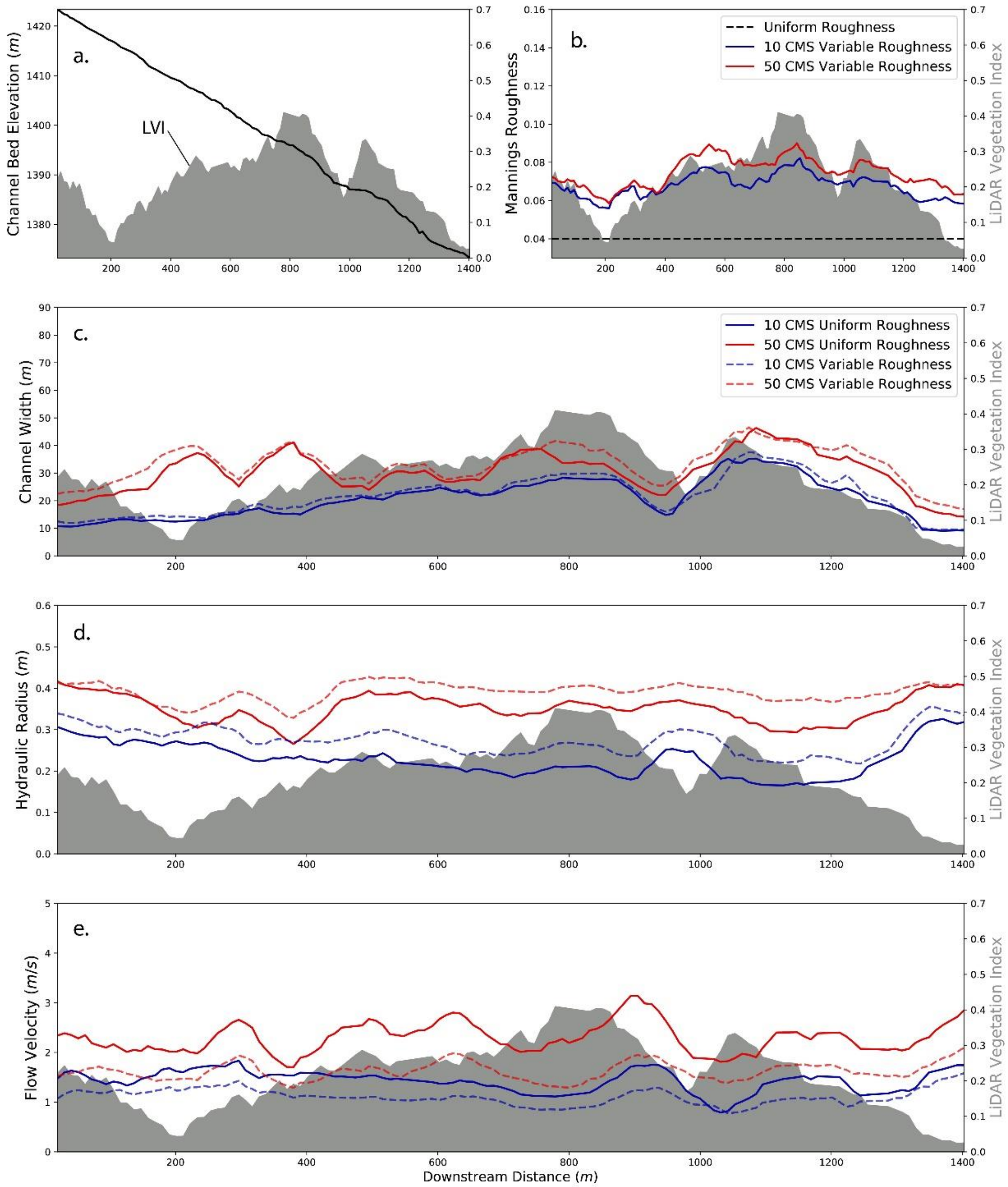

Figure 5: Upper Woodruff Canyon. Description of figure panels is otherwise the same as for Figure 4.

Figure 6

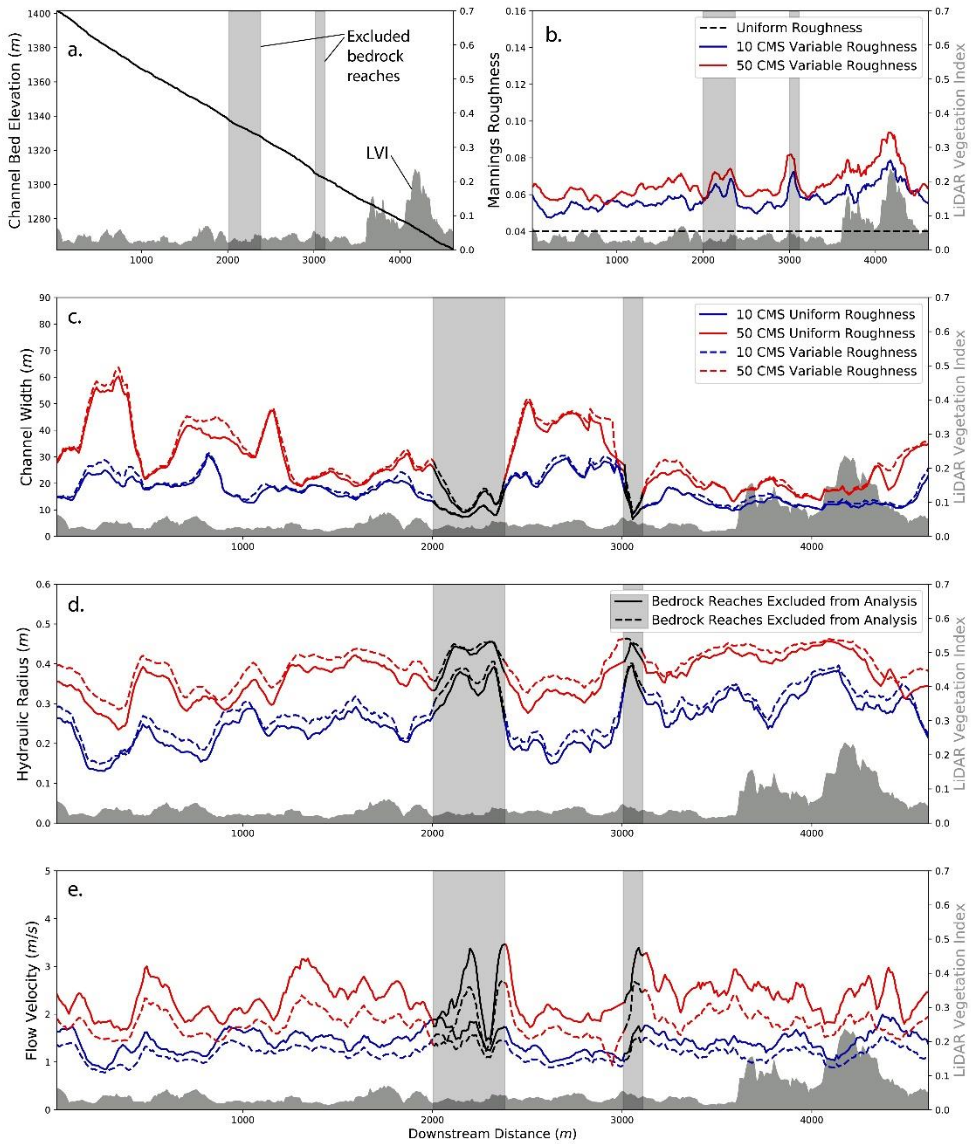

Figure 6: Trail Canyon. Bedrock reaches excluded from subsequent analyses represent narrow epigenetic gorge reaches where width appears controlled by bedrock walls and more recent bedrock incision (Ouimet et al., 2008), rather than being able to adjust by eroding alluvium. Description of figure panels is otherwise the same as for Figure 4.

Figure 7

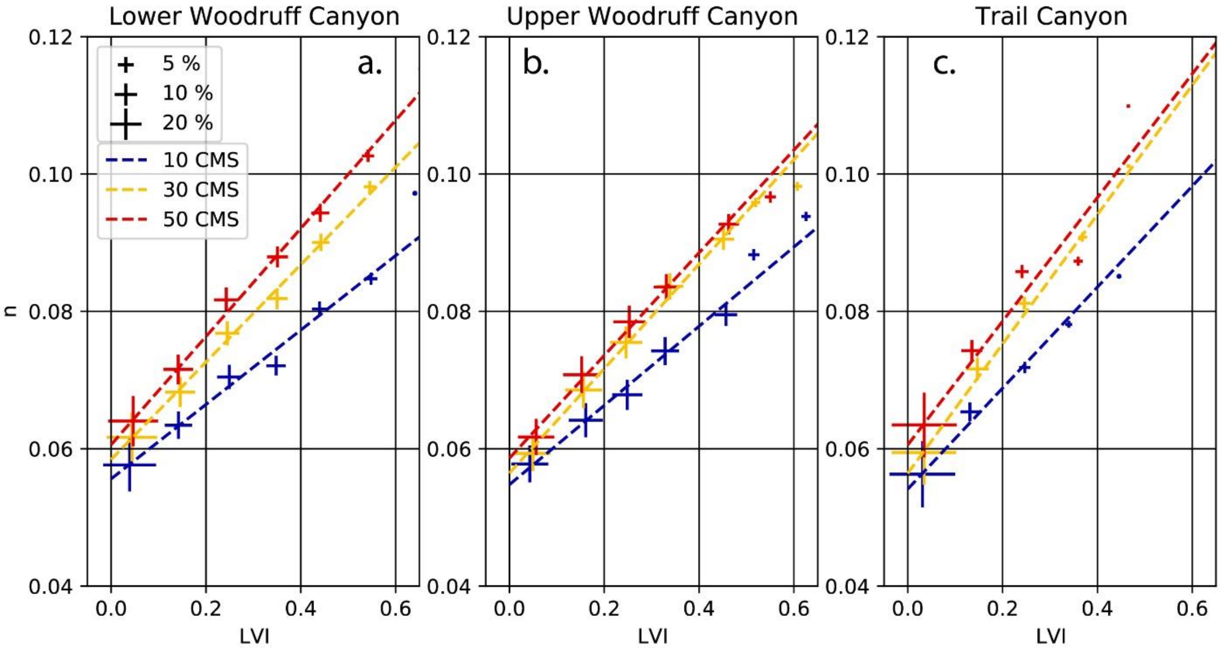

Figure 7: When calculated for the variable roughness case, Manning's n increases with LVI and also with discharge. Crosses represent averaged Manning's n for bins spanning 0.1 LVI, with their size indicating that bin's proportion of the overall dataset. For visual clarity, 20 and 40 m^3/s discharges are not shown. Dashed lines represent linear regressions.

Figure 8

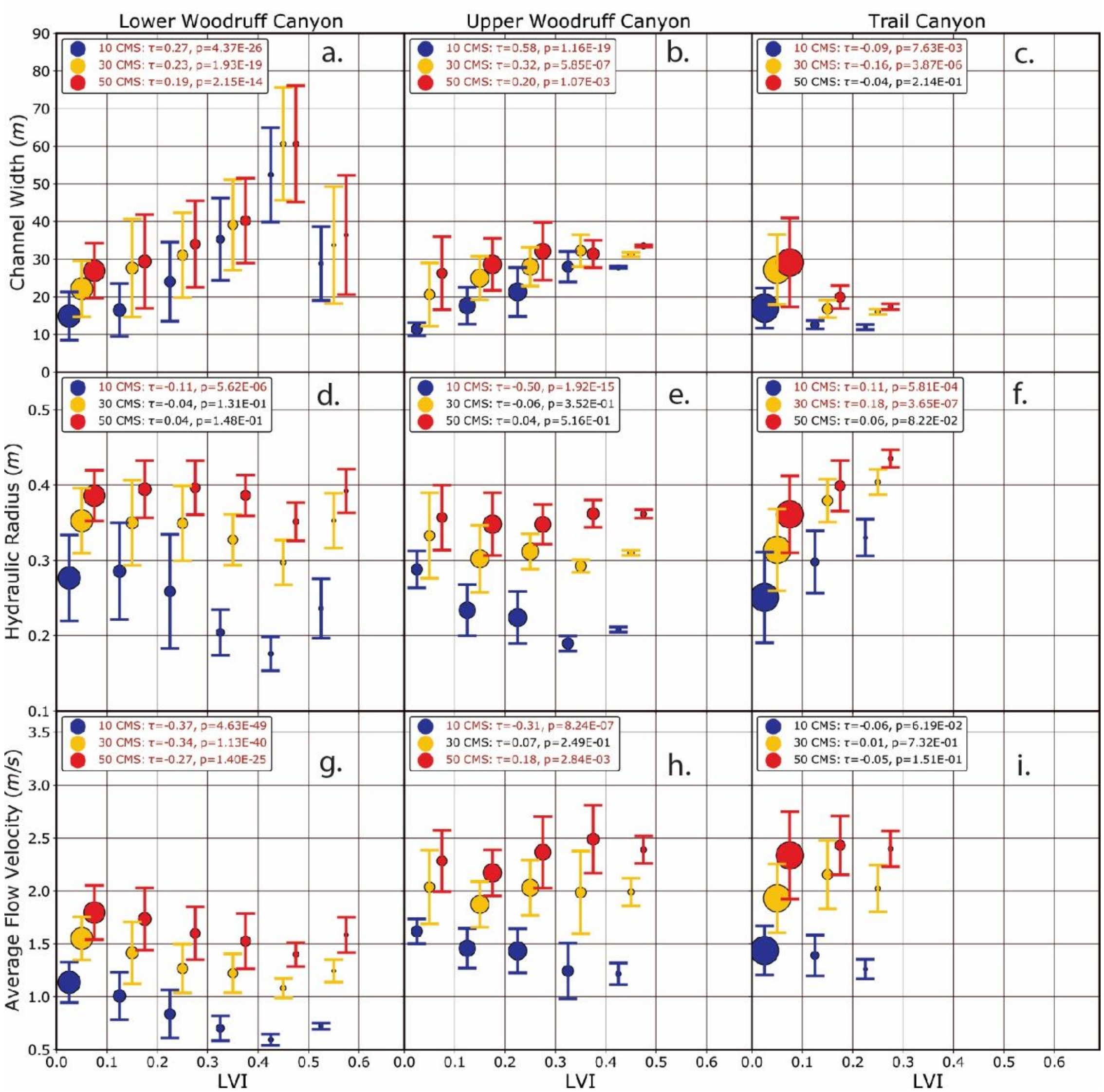

Figure 8: Correlations between LiDAR Vegetation Index and wetted width, hydraulic radius, and cross-section averaged velocity, at discharges of 10, 30, and 50 m^3/s, for uniform roughness models (n=0.04). Data are binned in LVI increments of 0.1 (0-0.1, 0.1-0.2, etc.). Data for 10 and 50 m^3/s are offset from the LVI bin centers (0.05, 0.15, etc.) for visual clarity. Whiskers span ±1 standard deviation. Size of points represents the relative proportion of data points in that bin. Legends show Kendall τ coefficient and associated p-values; statistically significant correlations (p<0.05) are highlighted in red.

Figure 9

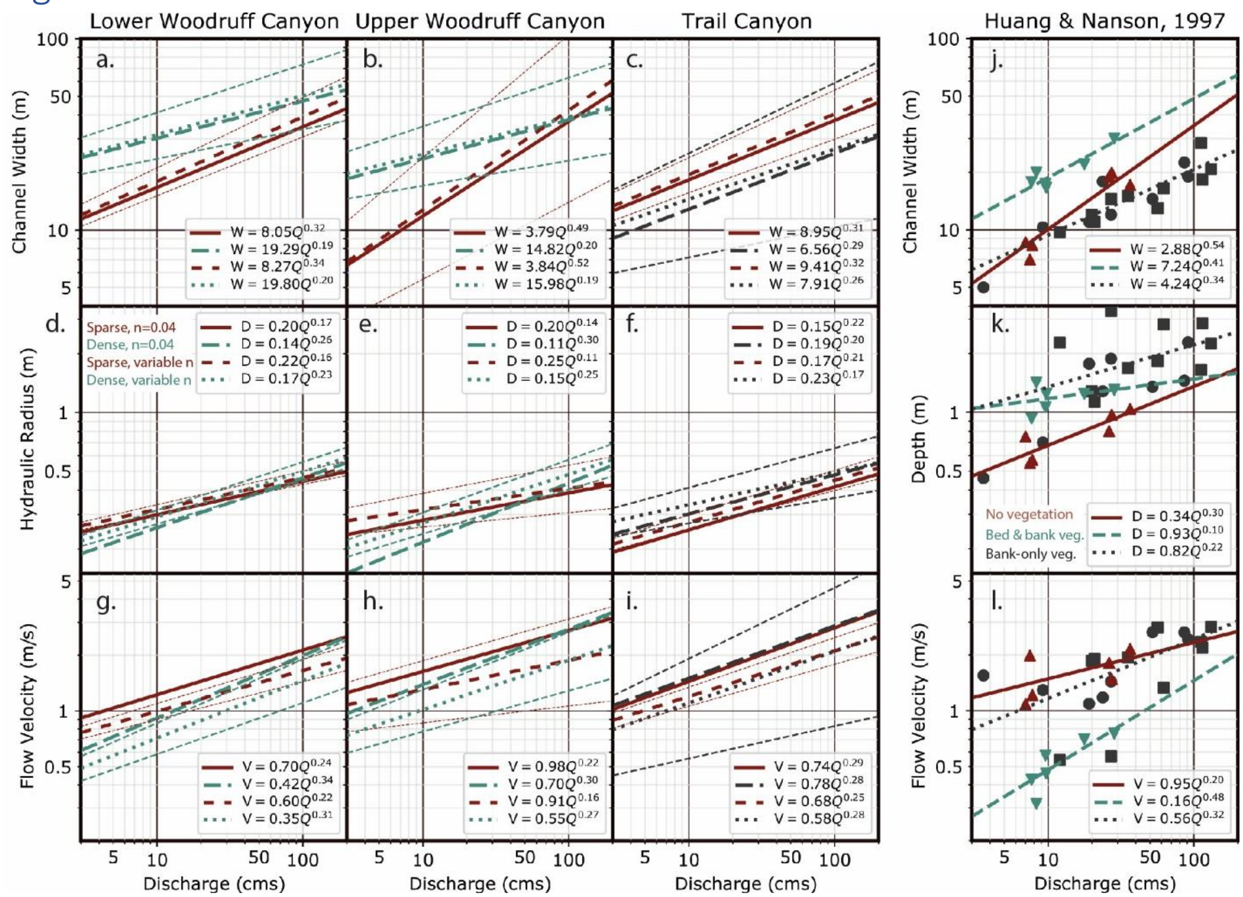

Figure 9a-i: Best-fit hydraulic geometry scaling for uniform hydraulic roughness and spatially variable hydraulic roughness, for data classified as sparsely- and densely-vegetated. The panel d legend (i.e, sparse and dense vegetation, uniform and variable n) applies to panels a-i. Data points are not shown in order to better visualize the relations among fits. Additional bounding lines visually indicate 95% confidence intervals on regression parameters (coefficient and exponent) for the variable roughness cases; uncertainties are similar for uniform roughness regressions. j-l. Huang and Nanson (1997) data and our regressions to them. Note that k reflects depth, while d,e,f reflect hydraulic radius.

Figure 10

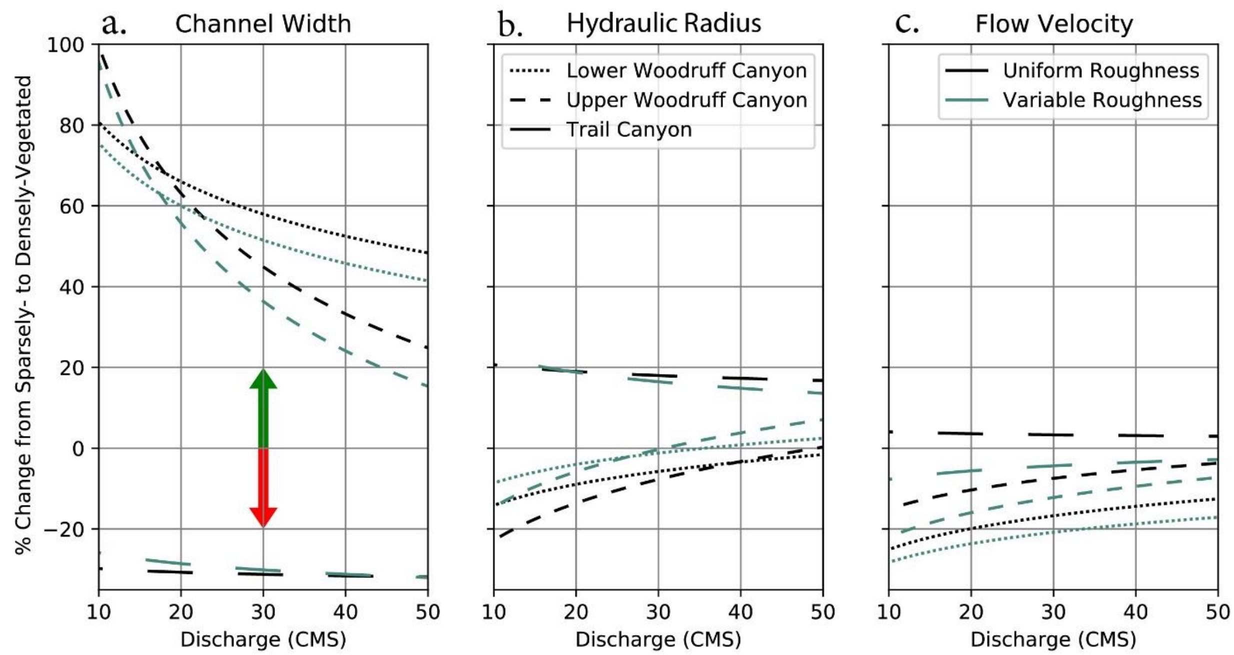

Figure 10: Percent change between sparsely- and densely-vegetated reaches in terms of channel (a) width, (b) hydraulic radius, and (c) flow velocity, over the range of discharges modeled in this study. Percent change was calculated from the regression curves shown in Figure 9, as the densely-vegetated curve minus the sparsely-vegetated curve divided by the sparsely-vegetated curve. Positive % change values (green arrow) indicate that the densely-vegetated case is larger that the sparsely-vegetated case. Negative values (red curve) indicate that the sparsely-vegetated case is larger. Along Trail canyon, for example, densely-vegetated reaches are ≈25% narrower than sparsely-vegetated reaches, and this difference is relatively insensitive to discharge. In contrast, for both Woodruff spring reaches, densely-vegetated widths are nearly double sparsely vegetated widths at low discharges. At higher discharges, densely-vegetated widths are ≈20 to 40% higher than sparsely-vegetated widths. Channel width (a) is more sensitive to vegetation than are hydraulic radius (b) or flow velocity (c).

Table 1: Flow modeling results with uniform and variable roughness

Channel	Modeled Q	n, avg. ± 1σ	Q, avg ± 1σ	LVI, avg. ± 1σ	Width, avg. ± 1σ	Hyd. Rad., avg. ± 1σ	Vel., avg. ± 1σ
Units	**m^3/s**	**$s/m^{1/3}$**	**m^3/s**	**-**	**m**	**m**	**m/s**
Lower	10	0.04	7.07 ± 0.39	0.14 ± 0.15	19.2 ± 12.3	0.27 ± 0.08	1.02 ± 0.34
Woodruff,	20	0.04	16.01 ± 0.78	0.14 ± 0.15	24.2 ± 14.1	0.31 ± 0.07	1.26 ± 0.38
n constant	30	0.04	26.24 ± 1.24	0.15 ± 0.15	27.4 ± 14.6	0.35 ± 0.06	1.44 ± 0.42
	40	0.04	36.63 ± 1.66	0.15 ± 0.15	29.5 ± 14.4	0.37 ± 0.05	1.59 ± 0.44
	50	0.04	47.38 ± 2.21	0.15 ± 0.15	31.2 ± 14.4	0.39 ± 0.04	1.71 ± 0.47
Lower	10	0.063 ± 0.010	7.30 ± 0.41	0.14 ± 0.15	21.0 ± 12.9	0.29 ± 0.07	0.82 ± 0.26
Woodruff,	20	0.067 ± 0.012	16.88 ± 0.83	0.15 ± 0.15	26.5 ± 14.4	0.34 ± 0.06	1.01 ± 0.28
n variable	30	0.069 ± 0.012	27.51 ± 1.29	0.15 ± 0.15	30.0 ± 14.8	0.38 ± 0.04	1.15 ± 0.30
	40	0.072 ± 0.013	38.18 ± 1.82	0.16 ± 0.15	32.3 ± 14.8	0.40 ± 0.04	1.26 ± 0.33
	50	0.073 ± 0.014	49.06 ± 2.28	0.16 ± 0.15	34.6 ± 14.9	0.41 ± 0.04	1.33 ± 0.35
Upper	10	0.04	9.72 ± 0.30	0.21 ± 0.15	20.0 ± 9.0	0.23 ± 0.05	1.44 ± 0.38
Woodruff,	20	0.04	20.11 ± 0.51	0.21 ± 0.15	22.8 ± 8.6	0.29 ± 0.05	1.82 ± 0.44
n constant	30	0.04	30.67 ± 0.73	0.21 ± 0.14	26.6 ± 9.5	0.31 ± 0.05	1.97 ± 0.52
	40	0.04	41.20 ± 1.10	0.21 ± 0.14	28.8 ± 10.3	0.33 ± 0.05	2.13 ± 0.55
	50	0.04	51.76 ± 1.47	0.21 ± 0.14	30.0 ± 10.4	0.35 ± 0.05	2.31 ± 0.56
Upper	10	0.067 ± 0.010	9.96 ± 0.3	0.22 ± 0.15	21.0 ± 8.7	0.28 ± 0.05	1.12 ± 0.26
Woodruff,	20	0.076 ± 0.011	20.39 ± 0.63	0.22 ± 0.14	25.0 ± 9.4	0.34 ± 0.04	1.31 ± 0.28
n variable	30	0.073 ± 0.012	31.09 ± 0.98	0.21 ± 0.14	28.0 ± 9.2	0.36 ± 0.04	1.45 ± 0.34
	40	0.074 ± 0.012	41.78 ± 1.35	0.21 ± 0.14	30.4 ± 9.5	0.38 ± 0.04	1.55 ± 0.33
	50	0.074 ± 0.011	52.41 ± 1.71	0.21 ± 0.14	32.7 ± 9.7	0.39 ± 0.04	1.63 ± 0.34
Trail,	10	0.04	9.29 ± 0.42	0.05 ± 0.06	16.6 ± 6.5	0.26 ± 0.07	1.43 ± 0.36
n constant	20	0.04	19.35 ± 1.00	0.06 ± 0.07	22.7 ± 8.8	0.29 ± 0.07	1.71 ± 0.44
	30	0.04	29.54 ± 1.39	0.06 ± 0.07	25.6 ± 10.7	0.32 ± 0.07	1.96 ± 0.53
	40	0.04	40.13 ± 1.80	0.06 ± 0.07	27.8 ± 11.8	0.35 ± 0.06	2.16 ± 0.55
	50	0.04	50.89 ± 2.70	0.06 ± 0.07	27.7 ± 12.9	0.37 ± 0.06	2.35 ± 0.66
Trail,	10	0.058 ± 0.007	9.33 ± 0.42	0.05 ± 0.06	17.7 ± 7.0	0.28 ± 0.07	1.18 ± 0.27
n variable	20	0.060 ± 0.008	19.56 ± 0.94	0.06 ± 0.07	24.4 ± 9.5	0.32 ± 0.06	1.38 ± 0.31
	30	0.062 ± 0.009	29.72 ± 1.36	0.06 ± 0.07	27.8 ± 11.6	0.35 ± 0.06	1.54 ± 0.36
	40	0.064 ± 0.009	39.88 ± 1.81	0.06 ± 0.07	29.8 ± 12.3	0.37 ± 0.05	1.67 ± 0.37
	50	0.066 ± 0.009	50.43 ± 2.83	0.06 ± 0.07	29.5 ± 13.4	0.40 ± 0.05	1.82 ± 0.46

σ is 1 standard deviation, calculated for valid cross sections for Manning's n, discharge, LVI, width, hydraulic radius, and velocity.

Table 2: Correlation between LVI and variables, measured by Kendall's τ

Channel	Modeled Q, m3/s	τ, n	p-value, n	τ, Width	p-value, Width	τ, Hydraulic Radius	p-value, Hydraulic Radius	τ, Velocity	p-value, Velocity
Lower	10			**0.27**	**4.37E-26**	**-0.11**	**5.62E-06**	**-0.37**	**4.63E-49**
Woodruff,	20			**0.23**	**1.24E-19**	**-0.08**	**2.49E-03**	**-0.34**	**5.54E-42**
n constant	30			**0.23**	**1.93E-19**	-0.04	1.31E-01	**-0.34**	**1.13E-40**
	40			**0.21**	**2.71E-16**	0.00	9.72E-01	**-0.32**	**6.44E-37**
	50			**0.19**	**2.15E-14**	0.04	1.48E-01	**-0.27**	**1.40E-25**
Lower	10	**0.64**	**8.19E-139**	**0.28**	**1.39E-27**	**-0.09**	**5.05E-04**	**-0.43**	**1.38E-63**
Woodruff,	20	**0.62**	**2.42E-129**	**0.23**	**6.65E-20**	0.00	8.85E-01	**-0.43**	**5.57E-64**
n variable	30	**0.66**	**4.80E-146**	**0.23**	**1.94E-19**	**0.05**	**4.45E-02**	**-0.45**	**9.44E-69**
	40	**0.68**	**1.20E-154**	**0.21**	**9.05E-17**	**0.11**	**2.37E-05**	**-0.40**	**7.40E-55**
	50	**0.69**	**2.57E-158**	**0.16**	**8.24E-10**	**0.20**	**1.81E-14**	**-0.30**	**2.97E-32**
Upper	10			**0.58**	**1.16E-19**	**-0.50**	**1.92E-15**	**-0.31**	**8.24E-07**
Woodruff,	20			**0.55**	**1.92E-18**	**-0.31**	**8.08E-07**	**-0.15**	**1.70E-02**
n constant	30			**0.32**	**5.85E-07**	-0.06	3.52E-01	0.07	2.49E-01
	40			**0.23**	**2.30E-04**	0.01	8.42E-01	**0.16**	**8.62E-03**
	50			**0.20**	**1.07E-03**	0.04	5.16E-01	**0.18**	**2.84E-03**
Upper	10	**0.77**	**2.19E-35**	**0.59**	**2.46E-21**	**-0.37**	**3.73E-09**	**-0.53**	**1.38E-17**
Woodruff,	20	**0.85**	**8.28E-44**	**0.61**	**4.88E-23**	**-0.29**	**2.90E-06**	**-0.43**	**4.17E-12**
n variable	30	**0.83**	**1.21E-41**	**0.29**	**2.55E-06**	**0.18**	**4.58E-03**	-0.05	4.09E-01
	40	**0.83**	**1.32E-40**	**0.17**	**4.97E-03**	**0.25**	**5.89E-05**	0.03	6.41E-01
	50	**0.83**	**8.57E-41**	**0.17**	**5.81E-03**	**0.28**	**6.12E-06**	-0.03	6.28E-01
Trail,	10			**-0.09**	**7.63E-03**	**0.11**	**5.81E-04**	-0.06	6.19E-02
n constant	20			**-0.18**	**1.01E-07**	**0.20**	**5.35E-09**	0.06	7.60E-02
	30			**-0.16**	**3.87E-06**	**0.18**	**3.65E-07**	0.01	7.32E-01
	40			**-0.15**	**1.11E-05**	**0.14**	**4.34E-05**	-0.02	5.50E-01
	50			-0.04	2.14E-01	0.06	8.22E-02	-0.05	1.51E-01
Trail,	10	**0.29**	**6.25E-19**	**-0.08**	**1.02E-02**	**0.13**	**1.01E-04**	**-0.12**	**1.37E-04**
n variable	20	**0.33**	**4.81E-22**	**-0.17**	**5.45E-07**	**0.18**	**1.19E-07**	-0.06	7.04E-02
	30	**0.33**	**8.70E-22**	**-0.14**	**3.63E-05**	**0.15**	**7.54E-06**	**-0.11**	**1.27E-03**
	40	**0.30**	**9.73E-18**	**-0.13**	**1.98E-04**	**0.13**	**2.08E-04**	**-0.12**	**6.63E-04**
	50	**0.25**	**1.82E-14**	-0.03	3.29E-01	**0.07**	**4.24E-02**	**-0.11**	**7.16E-04**

τ is Kendall's rank correlation coefficient, measured between LVI and the given variable.

p-values < 0.05 suggest likely statistical significance, and are shown in **bold**.

Table 3: Hydraulic geometry scaling factors and exponents

Channel	Metric	a, Sparsely-vegetated	b, Sparsely-vegetated	a, Densely-vegetated	b, Densely-vegetated
Lower	Width ($W=aQ^b$)	8.05	0.32	19.29	0.19
Woodruff,	Hyd. Rad. ($HR=aQ^b$)	0.20	0.17	0.14	0.26
n constant	Velocity ($V=aQ^b$)	0.70	0.24	0.42	0.34
Lower	Width ($W=aQ^b$)	8.27	0.34	19.80	0.20
Woodruff,	Hyd. Rad. ($HR=aQ^b$)	0.22	0.16	0.17	0.23
n variable	Velocity ($V=aQ^b$)	0.60	0.22	0.35	0.31
Upper	Width ($W=aQ^b$)	3.79	0.49	14.82	0.20
Woodruff,	Hyd. Rad. ($HR=aQ^b$)	0.20	0.14	0.11	0.30
n constant	Velocity ($V=aQ^b$)	0.98	0.22	0.70	0.30
Upper	Width ($W=aQ^b$)	3.84	0.52	15.98	0.19
Woodruff,	Hyd. Rad. ($HR=aQ^b$)	0.25	0.11	0.15	0.25
n variable	Velocity ($V=aQ^b$)	0.91	0.16	0.55	0.27
Trail,	Width ($W=aQ^b$)	8.95	0.31	6.56	0.29
n constant	Hyd. Rad. ($HR=aQ^b$)	0.15	0.22	0.19	0.20
	Velocity ($V=aQ^b$)	0.74	0.29	0.78	0.28
Trail,	Width ($W=aQ^b$)	9.41	0.32	7.91	0.26
n variable	Hyd. Rad. ($HR=aQ^b$)	0.17	0.21	0.23	0.17
	Velocity ($V=aQ^b$)	0.68	0.25	0.58	0.28